12-13-2019

Finite element analysis of the mechanisms of impact mitigation inherent to the North American bison (Bison bison) skull

Andrea Karen Persons

Finite element analysis of the mechanisms of impact mitigation inherent to the North American bison (Bison bison) skull

By

Andrea Karen Persons

A Thesis
Submitted to the Faculty of
Mississippi State University
in Partial Fulfillment of the Requirements
for the Degree of Master of Science
in Biomedical Engineering
in the Department of Agricultural and Biological Engineering

Mississippi State, Mississippi

December 2019

Finite element analysis of the mechanisms of impact mitigation inherent to the North American bison (Bison bison) skull

By

Andrea Karen Persons

Approved:

_____
Lauren B. Priddy
(Major Professor)

_____
Steven H. Elder
(Co-Major Professor/Graduate Coordinator)

_____
James Ryan Butler
(Committee Member)

_____
Matthew W. Priddy
(Committee Member)

_____
Jason M. Keith
Dean
Bagley College of Engineering

Name: Andrea Karen Persons

Date of Degree: December 13, 2019

Institution: Mississippi State University

Major Field: Biomedical Engineering

Major Professors: Lauren B. Priddy and Steven H. Elder

Title of Study: Finite element analysis of the mechanisms of impact mitigation inherent to the North American bison (Bison bison) skull

Pages in Study: 74

Candidate for Degree of Master of Science

North American bison (Bovidae: *Bison bison*) incur blunt impacts to the interparietal and frontal bones when they engage in head-to-head fights. To investigate the impact mitigation of these bones, a finite element analysis of the skull under loading conditions was performed. Based on anatomical and histological studies, the interparietal and frontal bones are both comprised of a combination of haversian and plexiform bone, and are both underlain by bony septa. Additionally, the interparietal bone is thicker than the frontal. Data regarding the mechanical properties of bison bone are scarce, but the results of a phylogenetic analysis infer that the material properties of the closely-related domestic cow bone are a suitable proxy for use in the FEA. Results of the FEA suggest that the thickness of the interparietal in conjunction with the bony septa may prevent focal stresses by helping to absorb and disperse the blunt impact energy about the skull.

ACKNOWLEDGEMENTS

I would like to thank my major professor, Dr. Lauren Priddy, co-major professor, Dr. Steven Elder, and committee members, Dr. Ryan Butler and Dr. Matthew Priddy. Not only did they take on this project midstream, but their guidance and insights have tremendously improved this project. I would also like to thank Dr. Youssef Hammi for his assistance with the finite element analyses. Dr. Mark Horstemeyer helped initiate the project, and his insights along the way have been invaluable. I would also like to thank Dr. Mac Alford for reviewing the phylogenetic analysis. Drs. Jeremiah Deang, Nayeon Lee, and Heechen Cho provided invaluable assistance in the development of the models. Dr. Alicia Olivier prepared the histology slides which provided much needed material properties. This project was greatly improved by discussions with Dr. Bob Linford. Stephen Horstemeyer helped obtain bone samples, and Avery Schemmel and Elizabeth Whitehurst also assisted in the development of the anatomical and finite element models. Finally, this project would not have been possible were it not for the generosity of the Red Gate Ranch in Poplarville, Mississippi, who donated a bison skull, and for the loan of a bison skull by Dr. Chris Conroy. Thank you all!

TABLE OF CONTENTS

LIST OF TABLES

LIST OF FIGURES

CHAPTER I

POTENTIAL TO REDUCE THE INCIDENCE OF BLUNT TRAUMA THROUGH THE INVESTIGATION OF NATURAL IMPACT MITIGATION SYSTEMS SUCH AS THE NORTH AMERICAN BISON (*BISON BISON*) SKULL

Traumatic injury is a global pandemic associated with high levels of morbidity and mortality among patients.[1] Globally, an estimated 300,000,000 healthy years of life are lost to injury, while the cost of inpatient treatment of trauma in the United States alone is an estimated $37.5 billion.[2–4] Traumatic injury often results from the transfer of kinetic energy to the patient as occurs during motor vehicle collisions (MVC) or while participating in sports;[1,5,6] therefore, interventions, such as improved materials and designs to increase the safety of vehicles and sports equipment, would reduce both the incidence and burden associated with trauma.

While injuries to the central nervous system and exsanguination are the leading causes of trauma-related deaths,[7–11] the long-term sequelae of trauma also contributes to the social, psychological, and economic costs of trauma beyond the initial inpatient care.[12] For example, recent publicity regarding the potential link between repetitive mild traumatic brain injury (mTBI) and subsequent neurodegeneration in American football players has raised awareness of the social burden imposed by traumatic injury,[13–17] but traumatic injuries to the chest, abdomen, and pelvis are no less detrimental. Blunt injuries to the chest may result in disruption of the electrical system of the heart (e.g. *commotio cordis*),[18–22] while blunt injuries to the chest, abdomen, and pelvis may result in fractures, compromise the vasculature, and result in damage to additional organs such as the lungs, liver, kidneys, intestines, and bladder resulting in an initial

abbreviated surgery to stop hemorrhaging and control infection followed by definitive fracture fixation and wound closure in subsequent surgeries.[23–35]

As bipeds with little external protection, humans are not designed to engage in behaviors that induce blunt trauma; however, other animals have anatomical features that allow them to withstand numerous blunt impact events. Recent research has focused on understanding how these anatomical features prevent traumatic injury and the potential to artificially mimic these features in the design of safety equipment.[36] For example, studies on the horn of a bighorn sheep ram (*Ovis canadensis*)[36] and the hyoid apparatus of a red-bellied woodpecker (*Melanerpes carolinus*)[37] suggest that the geometries of these features affect the dissipation of shockwaves produced during head impacts. In particular, the tapered spiral of the horn of a ram converts the longitudinal stress waves produced when the rams collide into shear waves and increases uniaxial deformation via the reduction in cross-sectional area.[36] Similarly, the energy produced by the drumming of the red-bellied woodpecker is dissipated as it travels along the spiraled hyoid bone by the conversion of longitudinal stress waves into shear waves.[37]

Like bighorn sheep, American bison (*Bison bison*) engage in headbutting behaviors; however, in bison, the impact is directly to the head and is not buffered by the horns (Fig. 1.1). Although the headbutting behaviors are well-documented,[38–41] little is known of how the energy produced during the collisions is dissipated; therefore, to investigate the mechanisms of energy dissipation inherent to the bison skull and how these mechanisms may be used to protect humans from blunt trauma, the anatomy and histology of the North American bison skull were investigated, and the results were used to inform a finite element (FE) model of bison skull under low-velocity impact conditions (i.e. headbutting).

Additionally, input regarding the mechanical properties of bison bone was also needed for the FE model; however, information regarding the mechanical properties of bison bone is scarce, and when coupled with difficulties obtaining a fresh bison skull, necessitated using the mechanical properties of bone from a closely-related species.

North American bison belong to Bovidae, a family that also includes species such as the European bison (*Bison bonasus*), the domestic and wild yak (*Bos grunniens* and *Bos mutus*, respectively), the gaur (*Bos gaurus*), the banteng (*Bos javanicus*), the kouprey (*Bos sauveli*), and domestic cattle (*Bos taurus*).[42–52] Of these species, the mechanical properties of domestic cattle bones have been extensively characterized;[53–65] therefore, a phylogenetic analysis and estimation of genetic divergence were used to determine if the mechanical properties of domestic cattle bone served as a suitable substitute for those of bison bone.

Figure 1.1 North American bison engaged in head-to-head contact. (Adobe Stock Photo)

References

1. Lecky FE, Bouamra O, Woodford M, Alexandrescu R, O'Brien SJ. Epidemiology of Polytrauma. In: Pape H-C, Peitzman AB, Schwab CW, Giannoudis PV, eds. *Damage Control Management in the Polytrauma Patient*. Springer; 2010:13-23.

2. Murray CJL, Vos T, Lozano R, et al. Disability-adjusted life years (DALYs) for 291 diseases and injuries in 21 regions, 1990–2010: a systematic analysis for the Global Burden of Disease Study 2010. *The Lancet*. 2012;380(9859):2197-2223. doi:10.1016/S0140-6736(12)61689-4

3. Shakur H, Roberts I, Piot P, Horton R, Krug E, Mersch J. A promise to save 100 000 trauma patients. *The Lancet*. 2012;380(9859):2062-2063. doi:10.1016/S0140-6736(12)62037-6

4. Velopulos CG, Enwerem NY, Obirieze A, et al. National cost of trauma care by payer status. *Journal of Surgical Research*. 2013;184(1):444-449. doi:10.1016/j.jss.2013.05.068

5. American College of Surgeons. *ATLS® Advanced Trauma Life Support® Student Course Manual*. 10th ed. American College of Surgeons; 2018.

6. Zetterberg H, Winblad B, Bernick C, et al. Head trauma in sports – clinical characteristics, epidemiology and biomarkers. *Journal of Internal Medicine*. 2019;285(6):624-634. doi:10.1111/joim.12863

7. Pfeifer R, Tarkin IS, Rocos B, Pape H-C. Patterns of mortality and causes of death in polytrauma patients—Has anything changed? *Injury*. 2009;40(9):907-911. doi:10.1016/j.injury.2009.05.006

8. Dutton RP, Stansbury LG, Leone S, Kramer E, Hess JR, Scalea TM. Trauma Mortality in Mature Trauma Systems: Are We Doing Better? An Analysis of Trauma Mortality Patterns, 1997–2008. *Journal of Trauma and Acute Care Surgery*. 2010;69(3):620. doi:10.1097/TA.0b013e3181bbfe2a

9. Lansink KWW, Gunning AC, Leenen LPH. Cause of death and time of death distribution of trauma patients in a Level I trauma centre in the Netherlands. *Eur J Trauma Emerg Surg*. 2013;39(4):375-383. doi:10.1007/s00068-013-0278-2

10. Oyeniyi BT, Fox EE, Scerbo M, Tomasek JS, Wade CE, Holcomb JB. Trends in 1029 trauma deaths at a level 1 trauma center: Impact of a bleeding control bundle of care. *Injury*. 2017;48(1):5-12. doi:10.1016/j.injury.2016.10.037

11. Jochems D, Leenen LPH, Hietbrink F, Houwert RM, van Wessem KJP. Increased reduction in exsanguination rates leaves brain injury as the only major cause of death in blunt trauma. *Injury*. 2018;49(9):1661-1667. doi:10.1016/j.injury.2018.05.012

12. Starr AJ. Posttraumatic Stress Disorder and Psychological Sequelae after Severe Trauma. In: Pape H-C, Sanders R, Borrelli, Jr. J, eds. *The Poly-Traumatized Patient with Fractures*. Springer; 2011:345-348.

13. Gavett BE, Stern RA, McKee AC. Chronic Traumatic Encephalopathy: A Potential Late Effect of Sport-Related Concussive and Subconcussive Head Trauma. *Clinics in Sports Medicine*. 2011;30(1):179-188. doi:10.1016/j.csm.2010.09.007

14. Baugh CM, Stamm JM, Riley DO, et al. Chronic traumatic encephalopathy: neurodegeneration following repetitive concussive and subconcussive brain trauma. *Brain Imaging and Behavior*. 2012;6(2):244-254. doi:10.1007/s11682-012-9164-5

15. McKee AC, Stein TD, Nowinski CJ, et al. The spectrum of disease in chronic traumatic encephalopathy. *Brain*. 2013;136(1):43-64. doi:10.1093/brain/aws307

16. Mez J, Daneshvar DH, Kiernan PT, et al. Clinicopathological Evaluation of Chronic Traumatic Encephalopathy in Players of American Football. *JAMA*. 2017;318(4):360-370. doi:10.1001/jama.2017.8334

17. Horstemeyer MF, Berthelson PR, Moore J, Persons AK, Dobbins A, Prabhu RK. A Mechanical Brain Damage Framework Used to Model Abnormal Brain Tau Protein Accumulations of National Football League Players. *Ann Biomed Eng*. August 2019. doi:10.1007/s10439-019-02294-1

18. Link MS, Maron BJ, VanderBrink BA, et al. Impact directly over the cardiac silhouette is necessary to produce ventricular fibrillation in an experimental model of commotio cordis. *J Am Coll Cardiol*. 2001;37(2):649-654.

19. Maron BJ, Ahluwalia A, Haas TS, Semsarian C, Link MS, Estes NAM. Global epidemiology and demographics of commotio cordis. *Heart Rhythm*. 2011;8(12):1969-1971. doi:10.1016/j.hrthm.2011.07.014

20. Maron BJ, Gohman TE, Kyle SB, Estes, III NAM, Link MS. Clinical Profile and Spectrum of Commotio Cordis. *JAMA*. 2002;287(9):1142-1146. doi:10.1001/jama.287.9.1142

21. Maron BJ, Link MS, Wang PJ, Estes NA. Clinical profile of commotio cordis: an under appreciated cause of sudden death in the young during sports and other activities. *J Cardiovasc Electrophysiol*. 1999;10(1):114-120.

22. Maron BJ, Poliac LC, Kaplan JA, Mueller FO. Blunt impact to the chest leading to sudden death from cardiac arrest during sports activities. *N Engl J Med*. 1995;333(6):337-342. doi:10.1056/NEJM199508103330602

23. Fitzharris M, Franklyn M, Frampton R, King Y, Morris A, Fildes B. Thoracic Aortic Injury in Motor Vehicle Crashes: The Effect of Impact Direction, Side of Body Struck, and Seat Belt Use. *The Journal of Trauma: Injury, Infection, and Critical Care*. 2004;57(3):582-590. doi:doi: 10.1097/01.TA.0000088015.83951.D0

24. Lombardo G, Pryor JP. Phase I: Abbreviated Surgery - General. In: Pape H-C, Peitzman AB, Schwab CW, Giannoudis PV, eds. *Damage Control Management in the Polytrauma Patient*. Springer; 2010:123-149.

25. Nast-Kolb D, Waydhas C, Ruchholtz S, Taeger G. Phase I: Abbreviated Surgery - Orthopedics. In: Pape H-C, Peitzman AB, Schwab CW, Giannoudis PV, eds. *Damage Control Management in the Polytrauma Patient*. Springer; 2010:155-171.

26. Braslow B, Schwab CW. Phase III: Second Operation Repair of All Injuries General and Orthopedic - General. In: Pape H-C, Peitzman AB, Schwab CW, Giannoudis PV, eds. *Damage Control Management in the Polytrauma Patient*. Springer; 2010:211-227.

27. Pape H-C, Giannoudis PV. Phase III: Second Operation Repair of All Injuries General and Orthopedic - Orthopedic. In: Pape H-C, Peitzman AB, Schwab CW, Giannoudis PV, eds. *Damage Control Management in the Polytrauma Patient*. Springer; 2010:229-238.

28. Fabian TC. Phase IV: Late Reconstruction Abdominal Wall Closure: Staged Management Technique. In: Pape H-C, Peitzman AB, Schwab CW, Giannoudis PV, eds. *Damage Control Management in the Polytrauma Patient*. Springer; 2010:239-247.

29. Redeker J, Vogt PM. Phase IV: Late Reconstruction: Reconstruction of Posttraumatic Soft Tissue Defects. In: Pape H-C, Peitzman AB, Schwab CW, Giannoudis PV, eds. *Damage Control Management in the Polytrauma Patient*. Springer; 2010:249-263.

30. Giannoudis PV, Tzioupis CC, Pape H-C. Pelvic Fractures in Polytrauma Patients. In: Pape H-C, Peitzman AB, Schwab CW, Giannoudis PV, eds. *Damage Control Management in the Polytrauma Patient*. Springer; 2010:299-314.

31. Leenen LPH, Moll FL. Vascular Injuries in Polytrauma Patients. In: Pape H-C, Peitzman AB, Schwab CW, Giannoudis PV, eds. *Damage Control Management in the Polytrauma Patient*. Springer; 2010:315-329.

32. Mommsen P, Krettek C, Hildebrand F. Chest Trauma: Classification and Influence on the General Management. In: Pape H-C, Sanders R, Borrelli, Jr. J, eds. *The Poly-Traumatized Patient with Fractures*. Springer; 2011:75-88.

33. Burlew CC, Moore EE. Abdominal Injuries: Indications for Surgery. In: Pape H-C, Sanders R, Borrelli, Jr. J, eds. *The Poly-Traumatized Patient with Fractures*. Springer; 2011:89-102.

34. Hak DJ, Nork SE. Management of Pelvic Ring Injuries. In: Pape H-C, Sanders R, Borrelli, Jr. J, eds. *The Poly-Traumatized Patient with Fractures*. Springer; 2011:103-114.

35. Pfister D, Heidenreich A. Urological Injuries in Polytrauma. In: Pape H-C, Sanders R, Borrelli, Jr. J, eds. *The Poly-Traumatized Patient with Fractures*. Srpinger; 2011:115-126.

36. Johnson KL, Trim MW, Horstemeyer MF, et al. Geometric Effects on Stress Wave Propagation. *J Biomech Eng*. 2014;136(2):021023-021023-12. doi:10.1115/1.4026320

37. Lee N, Horstemeyer MF, Prabhu R, et al. The geometric effects of a woodpecker's hyoid apparatus for stress wave mitigation. *Bioinspir Biomim*. 2016;11(6):066004. doi:10.1088/1748-3190/11/6/066004

38. McHugh T. Social behavior of the American buffalo (*Bison bison bison*). *Zoologica : scientific contributions of the New York Zoological Society*. 1958;43(1):1-40.

39. Fuller WA. Behaviour and Social Organization of the Wild Bison of Wood Buffalo National Park, Canada. *1*. 1960;13(1):2-19. doi:10.14430/arctic3685

40. Lott DF. Sexual and Aggressive Behavior of Adult Male American Bison (*Bison bison*) in The Behaviour of Ungulates and its relation to management. *IUCN Publications new series*. 1974;I(24):382-394.

41. Lott DF. *American Bison, A Natural History*. University of California Press; 2002.

42. Hartl GB, Göltenboth R, Grilltsch M, Willing R. On the biochemical systematics of the bovini. *Biochemical Systematics and Ecology*. 1988;16(6):575-579. doi:10.1016/0305-1978(88)90065-8

43. Polziehn RO, Strobeck C, Sheraton J, Beech R. Bovine mtDNA Discovered in North American Bison Populations. *Conservation Biology*. 1995;9(6):1638-1638. doi:10.1046/j.1523-1739.1995.09061638.x

44. Hassanin A, Ropiquet A. Molecular phylogeny of the tribe Bovini (Bovidae, Bovinae) and the taxonomic status of the Kouprey, Bos sauveli Urbain 1937. *Molecular Phylogenetics and Evolution*. 2004;33(3):896-907. doi:10.1016/j.ympev.2004.08.009

45. Verkaar ELC, Nijman IJ, Beeke M, Hanekamp E, Lenstra JA. Maternal and paternal lineages in cross-breeding bovine species. Has wisent a hybrid origin? *Mol Biol Evol*. 2004;21(7):1165-1170. doi:10.1093/molbev/msh064

46. Nijman IJ, Boxtel DCJV, Cann LMV, Marnoch Y, Cuppen E, Lenstra JA. Phylogeny of Y chromosomes from bovine species. *Cladistics*. 2008;24(5):723-726. doi:10.1111/j.1096-0031.2008.00201.x

47. Douglas KC, Halbert ND, Kolenda C, Childers C, Hunter DL, Derr JN. Complete mitochondrial DNA sequence analysis of *Bison bison* and bison-cattle hybrids: function and phylogeny. *Mitochondrion*. 2011;11(1):166-175. doi:10.1016/j.mito.2010.09.005

48. Zeyland J, Wolko L, Lipiński D, et al. Tracking of wisent-bison-yak mitochondrial evolution. *J Appl Genet*. 2012;53(3):317-322. doi:10.1007/s13353-012-0090-4

49. Bibi F. A multi-calibrated mitochondrial phylogeny of extant Bovidae (Artiodactyla, Ruminantia) and the importance of the fossil record to systematics. *BMC Evol Biol*. 2013;13:166. doi:10.1186/1471-2148-13-166

50. Hassanin A, An J, Ropiquet A, Nguyen TT, Couloux A. Combining multiple autosomal introns for studying shallow phylogeny and taxonomy of Laurasiatherian mammals: Application to the tribe Bovini (Cetartiodactyla, Bovidae). *Mol Phylogenet Evol*. 2013;66(3):766-775. doi:10.1016/j.ympev.2012.11.003

51. Palacio P, Berthonaud V, Guérin C, et al. Genome data on the extinct Bison schoetensacki establish it as a sister species of the extant European bison (*Bison bonasus*). *BMC Evolutionary Biology*. 2017;17(1):48. doi:10.1186/s12862-017-0894-2

52. Hassanin A, Douzery EJP. Molecular and Morphological Phylogenies of Ruminantia and the Alternative Position of the Moschidae. *Systematic Biology*. 2003;52(2):206.

53. Currey JD. The effects of strain rate, reconstruction and mineral content on some mechanical properties of bovine bone. *Journal of Biomechanics*. 1975;8(1):81-86. doi:10.1016/0021-9290(75)90046-9

54. Reilly DT, Burstein AH. The elastic and ultimate properties of compact bone tissue. *Journal of Biomechanics*. 1975;8(6):393-405. doi:10.1016/0021-9290(75)90075-5

55. Van Buskirk WC, Cowin SC, Ward RN. Ultrasonic measurement of orthotropic elastic constants of bovine femoral bone. *J Biomech Eng*. 1981;103(2):67-72. doi:10.1115/1.3138262

56. Katz JL, Meunier A. The elastic anisotropy of bone. *Journal of Biomechanics*. 1987;20(11):1063-1070. doi:10.1016/0021-9290(87)90024-8

57. Sasaki N, Ikawa T, Fukuda A. Orientation of mineral in bovine bone and the anisotropic mechanical properties of plexiform bone. *Journal of Biomechanics*. 1991;24(1):57-61. doi:10.1016/0021-9290(91)90326-I

58. Martin RB, Boardman DL. The effects of collagen fiber orientation, porosity, density, and mineralization on bovine cortical bone bending properties. *Journal of Biomechanics*. 1993;26(9):1047-1054. doi:10.1016/S0021-9290(05)80004-1

59. Currey JD. The many adaptations of bone. *Journal of Biomechanics*. 2003;36(10):1487-1495. doi:10.1016/S0021-9290(03)00124-6

60. Locke M. Structure of long bones in mammals. *Journal of Morphology*. 2004;262(2):546-565. doi:10.1002/jmor.10282

61. Kim JH, Niinomi M, Akahori T, Toda H. Fatigue properties of bovine compact bones that have different microstructures. *International Journal of Fatigue*. 2007;29(6):1039-1050. doi:10.1016/j.ijfatigue.2006.09.018

62. Novitskaya E, Chen P-Y, Lee S, et al. Anisotropy in the compressive mechanical properties of bovine cortical bone and the mineral and protein constituents. *Acta Biomaterialia*. 2011;7(8):3170-3177. doi:10.1016/j.actbio.2011.04.025

63. Manilay Z, Novitskaya E, Sadovnikov E, McKittrick J. A comparative study of young and mature bovine cortical bone. *Acta Biomaterialia*. 2013;9(2):5280-5288. doi:10.1016/j.actbio.2012.08.040

64. Mayya A, Banerjee A, Rajesh R. Mammalian cortical bone in tension is non-Haversian. *Scientific Reports*. 2013;3:2533. doi:10.1038/srep02533

65. Dall'Ara E, Grabowski P, Zioupos P, Viceconti M. Estimation of local anisotropy of plexiform bone: Comparison between depth sensing micro-indentation and Reference Point Indentation. *Journal of Biomechanics*. 2015;48(15):4073-4080. doi:10.1016/j.jbiomech.2015.10.001

CHAPTER II

ANATOMY AND HISTOLOGY OF THE NORTH AMERICAN BISON (*BISON BISON*) SKULL

2.1 Introduction

When North American bison (*Bison bison*) engage in headbutting behaviors, contact is typically made along the caudal border of the frontal bone and the interparietal bone[1] (Figs. 1.1 and 2.1), but a paucity of data exists regarding the internal structure and histology of the bison skull. Studies of bison anatomy have focused on the archaeology of fossil bison bones,[2,3] the headbutting behavior itself,[4–7] or a study of the bison brain.[8]

Similar to the domestic cow, the outer skull of the bison is comprised of paired incisive, nasal, frontal, maxilla, lacrimal, and zygomatic bones and the singular interparietal bone.[9,10] (Fig.2.1). The external anatomy of the bison skull, however, provides little insight into how the frontal and interparietal bones dissipate the energy produced during headbutting which suggests that an underlying bony support structure that works with the frontal and interparietal bones to dissipate energy may be present.

Based on developmental biological studies of the fetal bovine skull, ossification of the frontal bones occurs between days 45 and 52 of gestation, and by day 97, the *substantia corticalis*, a thin area of cortical bone underlain by thin trabeculae that help distribute dynamic pressures, has developed.[11,12] As the fetus continues to develop, the nasal mucosa inverts into the trabeculae underlying the frontal bones to form the paranasal sinuses. After birth, the paranasal

sinuses continue to develop and eventually extend to underlie the frontal and interparietal bones.[9] The paranasal sinuses are separated by septa formed from bone and membranous tissue. These septa vary not only in their geometries, sizes, and angles, but are also variable among individuals.[9,13]

The interparietal bone in embryonic bovines arises from four ossification centers with ossification occurring between days 60 and 117 of gestation.[11,12,14] Developed in the absence of cartilage, the interparietal is a solid, wedge-shaped, thick bone that is also underlain by the paranasal sinuses.[9,11,12] Despite developmental studies of the bovine skull, the histology of the bones, especially that of the paranasal septa remain poorly characterized.

Three main bone types have been recognized in bovid skeletons and include, 1) haversian or cortical bone, 2) cancellous or trabecular bone, and 3) plexiform or fibrolamellar bone. Additionally, a combination of haversian and plexiform bone has also been observed in North American bison and domestic cattle.[15–19]

Cortical bone is dense, low-porosity bone comprised of osteons oriented along the longitudinal axis of the bone. Each osteon contains a central haversian canal encompassed by concentric lamellae and is differentiated from adjacent osteons by the presence of a cement line. The individual osteons are, however, linked by Volkmann's canals which help in the perfusion of the bone.[20] Conversely, cancellous bone is comprised of a highly porous lattice of plate and rod-shaped trabeculae which orient along the axes of principal stress for each bone. The open structure of cancellous bone allows for infilling with marrow bearing hematopoietic cells.[19,20] Plexiform bone, which contains interconnected vascular plexuses, is typically found in large, rapidly growing animals and is comprised of lamellar bone underlain by a core of woven bone creating a brick and mortar-type appearance.[19,21,22] (Fig. 2.2).

The mechanical properties also vary among bone types. Cortical bone behaves as transversely isotropic material, cancellous bone is anisotropic in nature, and plexiform bone behaves as an orthotropic material.[23,24] Plexiform bone is stiffer than cortical, and depending on its anatomical location within the bone, may have a higher elastic modulus. Further, plexiform bone tends to have a higher percentage of porosity than that of cortical due to the numerous vascular plexuses (Table 2.1).[15,23]

As the internal anatomy and bony composition of the North American bison skull are poorly characterized, a computed tomography (CT) of the skull of a four-year-old bison bull was completed, and samples from the frontal and interparietal bones from a three-year-old bison cow were collected and stained for microscopy. The information obtained from these studies was then used to inform a finite element model of bison headbutting.

2.2 Materials and Methods

2.2.1 Anatomical Characterization

As bovines are considered mature at age two,[25,26] a CT scan was performed on the skull of a four-year-old North American bison bull collected from the National Bison Range, Montana. The skull was loaned by the Museum of Vertebrate Zoology at the University of California, Berkeley (Accession number Mamm 99970). DICOM (Digital Images and Communication in Medicine) image files produced by the CT scan were then read in Simpleware™ ScanIP (N-2018.03-SP2 Build 55) and used to create a three-dimensional (3D) model of the skull that was composed of 5,186,280 triangular elements (Fig. 2.3). To examine the internal anatomy underlying the frontal and interparietal bones, the 3D model was then halved along the interfrontal suture that separates the two frontal bones. The incisive and nasal

bones along with the diffusive nasal tissue were then removed to further facilitate visualization of the internal structures of the frontal and interparietal bones reducing the number of triangular elements to 845,460 (Fig. 2.4).

2.2.2 Histological Characterization

Using a Dremel tool, rectangular bone samples (24.5 mm x 12.25) were taken from the frontal and interparietal bones of the dried skull of the three-year-old ranch-raised female bison donated by the Red Gate Ranch, Poplarville, Mississippi. The samples were soaked in phosphate-buffered saline (PBS) for 24 hours, and subsequently preserved in 10% formalin. Samples were then sectioned, mounted on slides, and stained with hematoxylin and eosin (H&E) at the Pathobiology and Population Medicine Lab, College of Veterinary Medicine, Mississippi State University. The slides were then examined and imaged with both brightfield and polarized microscopy using a total magnification of 100x (10x ocular • 10x objective). Selected areas from two of the brightfield images were subsequently analyzed using the jPOR[27] macro available for ImageJ[28] to determine the porosity of the samples. The selected areas were chosen to minimize the transection of any pores by the border of the area.

2.3 Results

2.3.1 Anatomical Characterization

Based on the 5,186,280 element model, the total length of the male skull (tip of the incisive – mid-interpariatal) is approximatly 526.4 mm, while the maximum width of the skull (outer right orbital – outer left orbital) is approximately 331.2 mm.

Reviewing the 845,460 element 3D model of the male bison skull, the frontal and interparietal bones have an average thickness of 8.9 mm and 19.6 mm, respectively (Fig. 2.5). The thickness of the frontal bone varies along its length and is thickest about the middle (midfrontal). Within the midfrontal region, an average thickness of 14.6 mm was recorded. The average inner distance between the outer and inner tables of the frontal bone is approximately 33.0 mm. Both the outer table of the frontal bone and the interparietal bone are underlain by the paranasal sinuses which are separated by bony septa of various geometries and sizes. Some septa connect the outer table of the frontal bone to its inner table. The paranasal sinuses overlie the braincase.

2.3.2 Histological Characterization

Images from both the brightfield and polarized microscopy of the H&E stained slides reveal the presence of bone comprised of both haversian and plexiform bone. The haversian bone is characterized by the presence of osteons encompassed by circumferential lamellae, while the plexiform bone is characterized by the linear lamellae above, between, and below the osteons (Fig. 2.6). Based on the image analysis, the porosity of the samples ranges from approximately 4.9 – 6.0% (Fig. 2.7).

2.4 Discussion and Conclusions

Similar to the findings of other research on bovine bone, a combination of haversian and plexiform bone was identified in the bison skull.[15,17,18] The porosity range of approximately 4.9% - 6.0% obtained from the image analysis of the brightfield images is also similar the 5.8% identified in previous research (Table 2.1).[15] Anatomically, the interparietal bone was found to be thicker than that of the frontal bone. It is unknown whether the increased thickness of the

interparietal bone is present at birth or whether it conforms to Wolff's Law and thickens as a result of bone remodeling resulting from microcrack development during headbutting. The effect of the thickness of the interparietal bone along with the presence of the bony septa underlying the frontal and interparietal bones on impact energy mitigation was explored using a finite element analysis using the material properties of combined haversian and plexiform bone.

Table 2.1
Selected Properties of Bovine Bone

	Elastic Modulus (GPa)	Ultimate Strength (MPa)	Porosity (%)
Cortical	17.5[29] 18.63 ± 1.21[15]	217.1 + 15.7[15]	4.9[15]
Plexiform	26.5[29] 21.02 ± 1.89[15]	230.5 + 17.7[15] 294[30]	6.4[15]

Haversian + Plexiform	10.95 ± 1.45[15] 12.4 ± 0.4[18]	223.8 ± 19.4[15]	5.8[15]

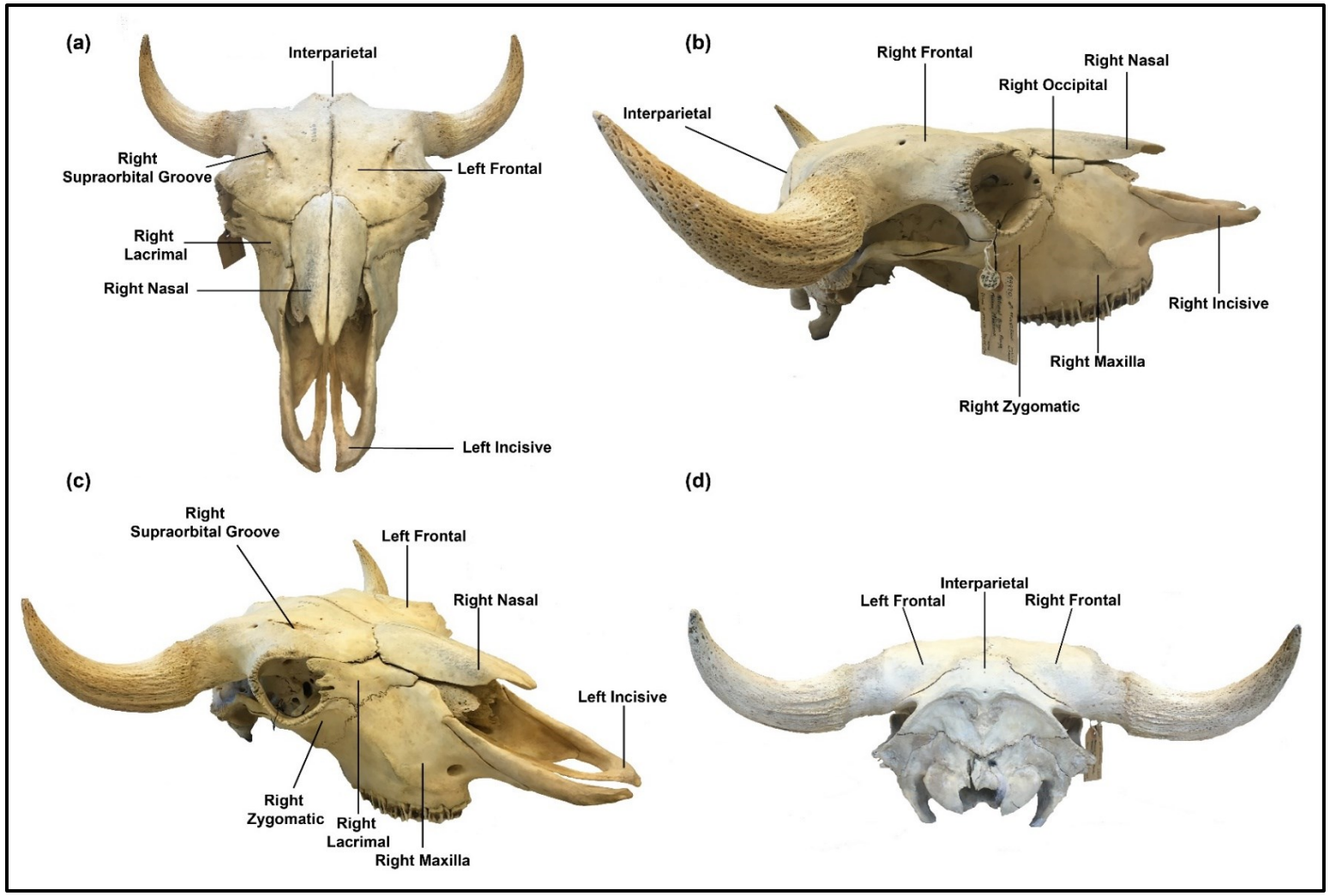

Figure 2.1 Outer anatomy of the four-year-old North American bison bull skull. (a) Rostral view, (b) Lateral view, (c) Oblique view, and (d) caudal view

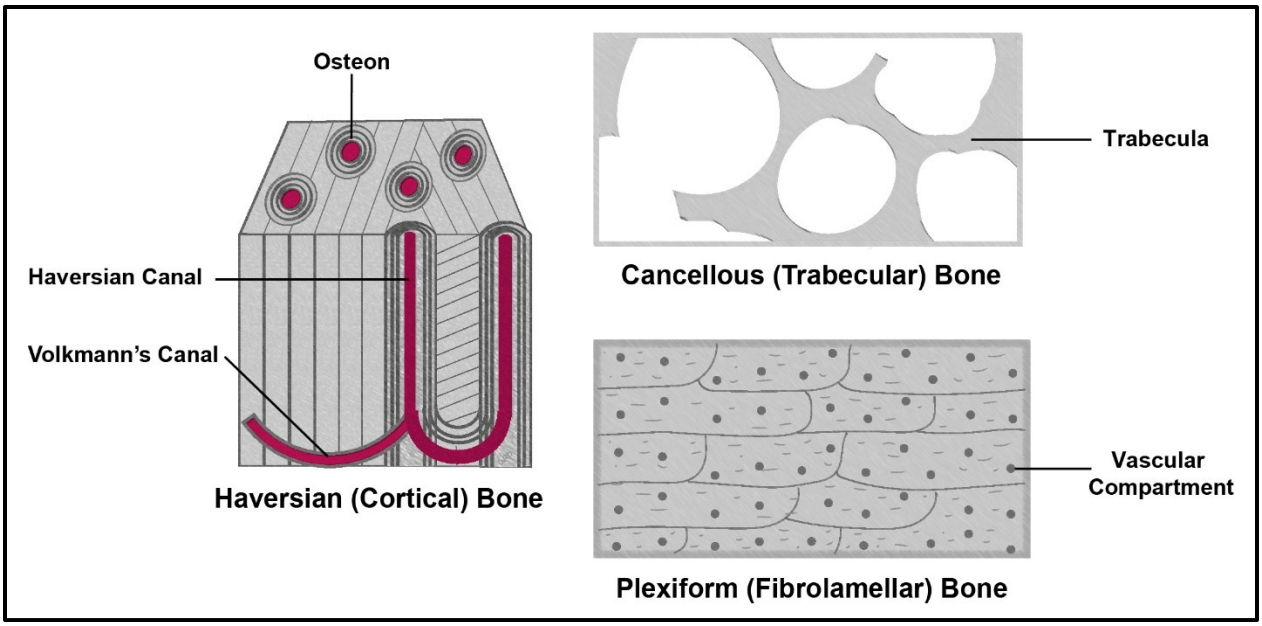

Figure 2.2 Haversian, cancellous, and plexiform bone are the three main bone types found in North American bison.

Figure 2.3 Three-dimensional model of the skull of the four-year-old bison bull. The model is composed of 5,186,280 triangular elements.

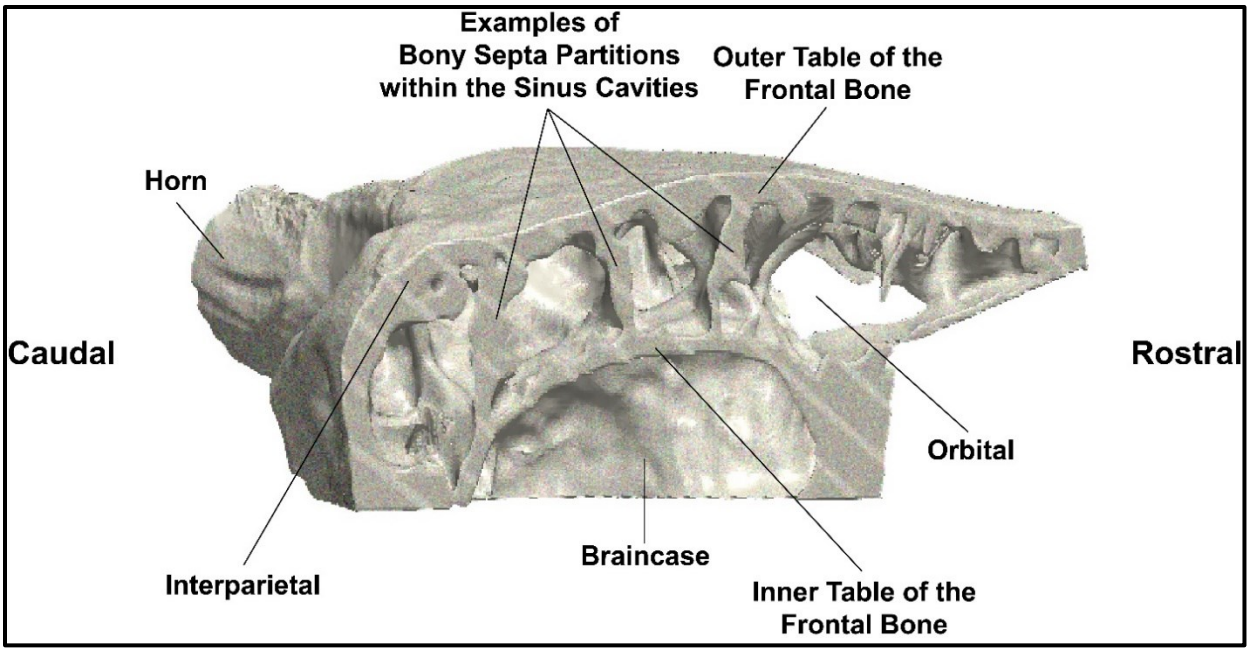

Figure 2.4 Internal anatomy underlying the frontal and interparietal bones of the skull of the four-year-old bison bull. The 3D model is comprised of 845,460 triangular elements.

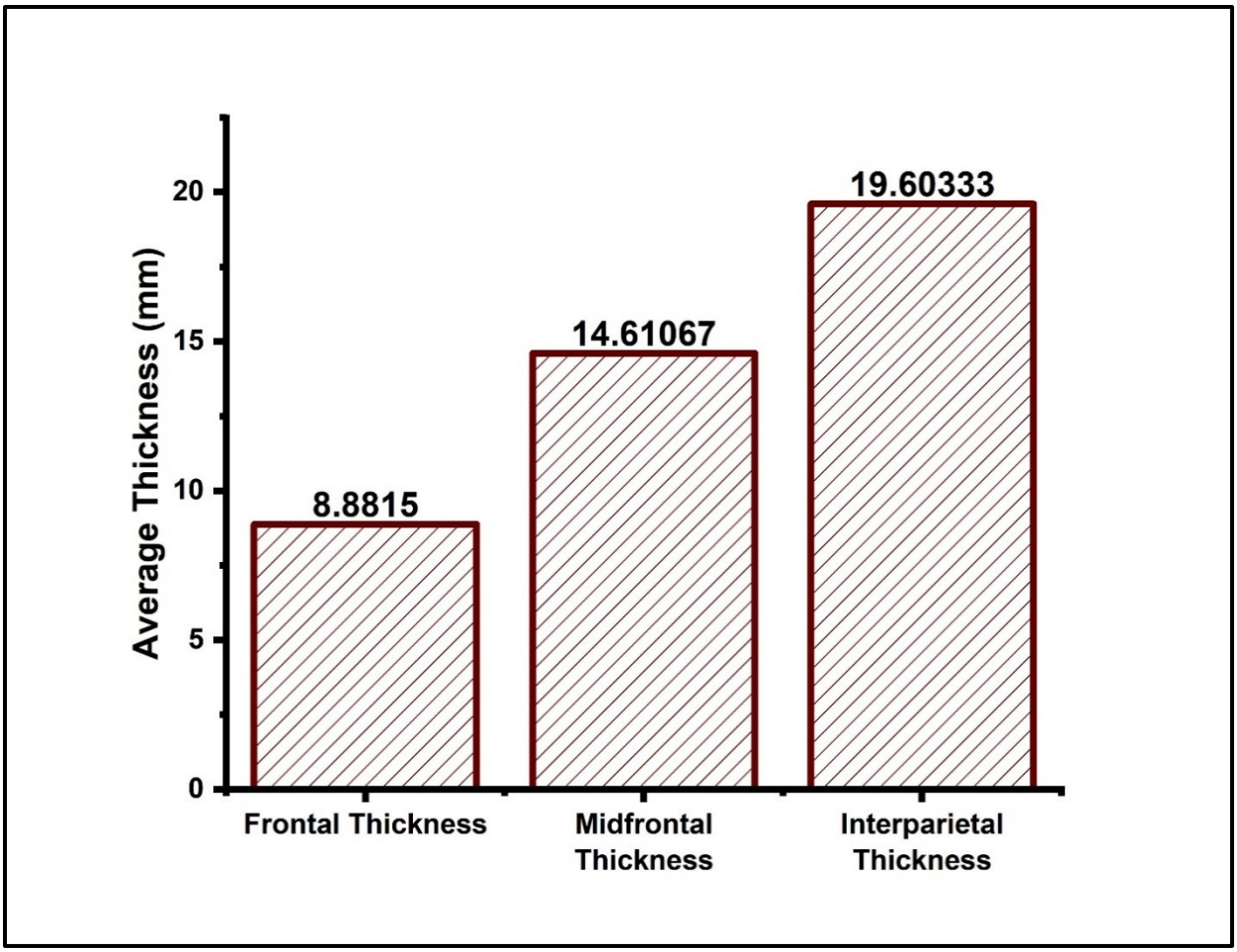

Figure 2.5 Histogram of the average thicknesses of the frontal bone, midfrontal region, and interparietal bones from the skull of the four-year-old bison bull.

The average values (in mm) are given above the bars.

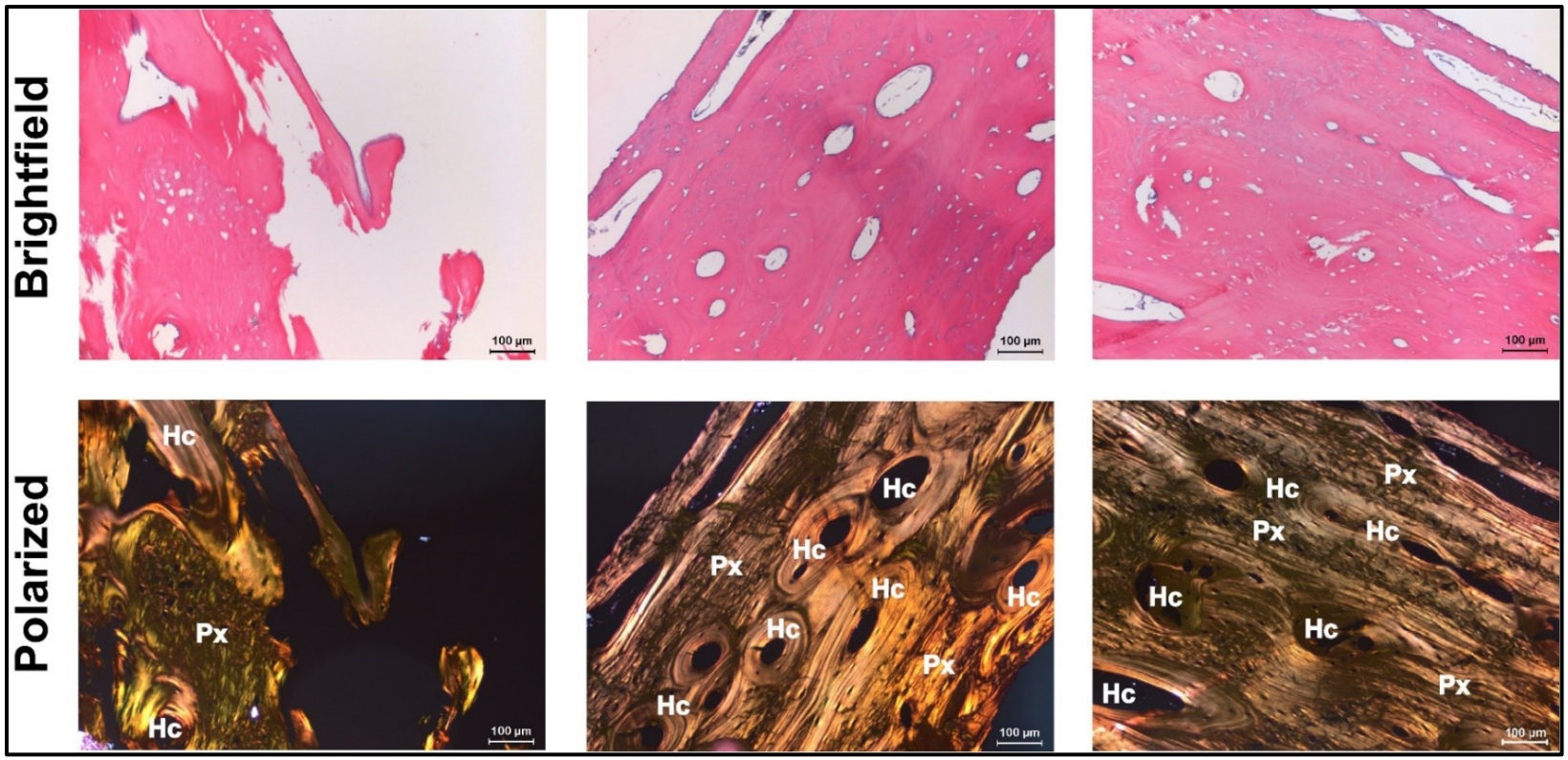

Figure 2.6 Images from brightfield and polarized microscopy of samples from the frontal and interparietal bison bones. Both Haversian (Hc) and Plexiform (Px) bone are present.

As the samples were taken from dried bone, the nuclei are no longer present in the bone.

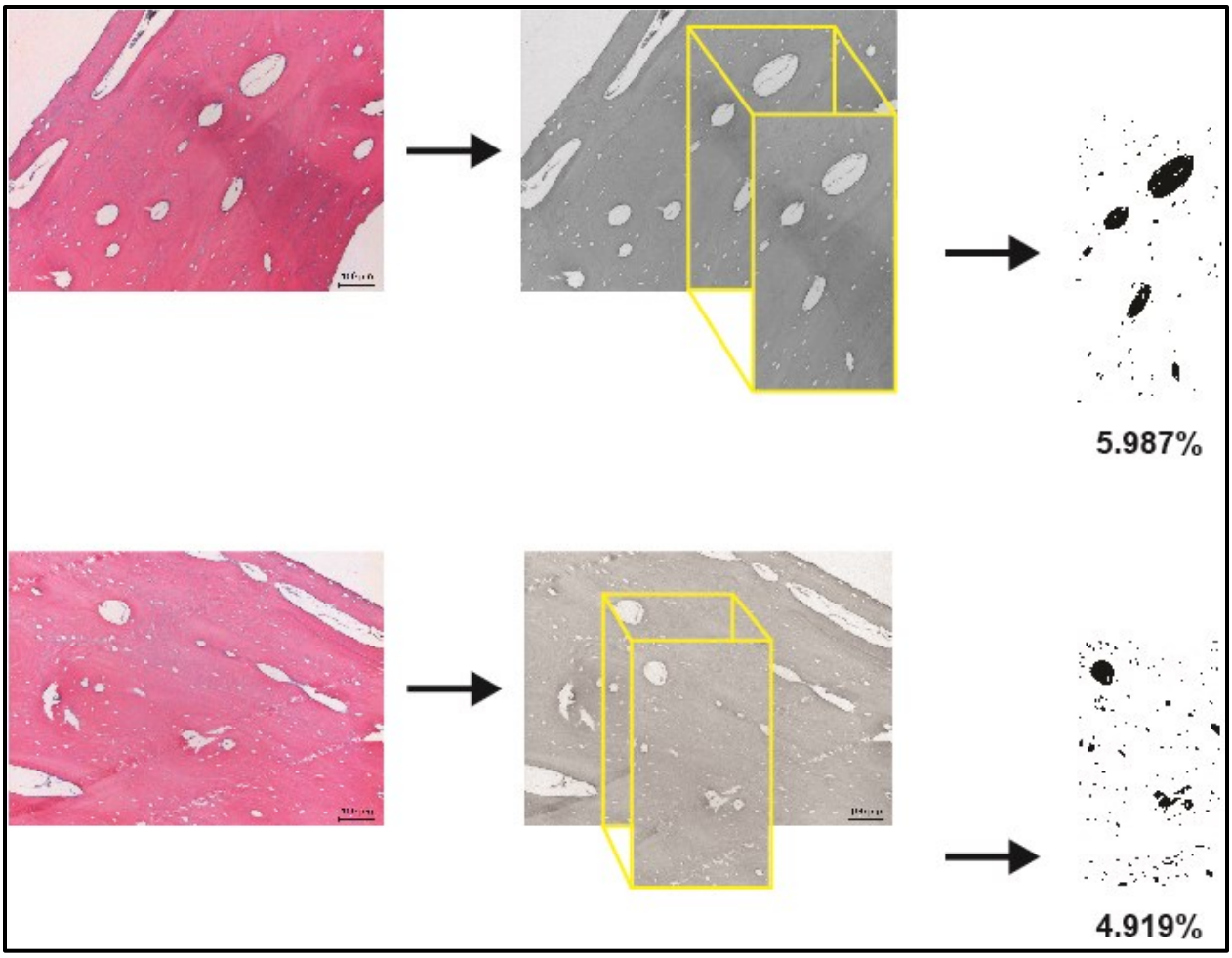

Figure 2.7 Example of the steps involved in determining the porosity of the combination of haversian and plexiform bone identified in the bison cow skull.

The brightfield images are converted black and white photos, and the areas where pores will not be transected by the borders are selected for analysis. A threshold is applied, and the porosity percentage is calculated based on the number of pixels comprising the pores divided by the total number of pixels in the selected areas.[27,28]

References

1. Kreutzer LA. Bison and deer bone mineral densities: Comparisons and implications for the interpretation of archaeological faunas. *Journal of Archaeological Science*. 1992;19(3):271-294. doi:10.1016/0305-4403(92)90017-W

2. Skinner MF, Kaisen OC. The fossil bison of Alaska and preliminary revision of the genus. Bulletin of the AMNH ; v. 89, article 3. 1947. http://digitallibrary.amnh.org/handle/2246/399. Accessed July 9, 2018.

3. Gilbert BM. *Mammalian Osteology*. Missouri Archaeological Society; 1990.

4. McHugh T. Social behavior of the American buffalo (*Bison bison bison*). *Zoologica : scientific contributions of the New York Zoological Society*. 1958;43(1):1-40.

5. Fuller WA. Behaviour and Social Organization of the Wild Bison of Wood Buffalo National Park, Canada. *1*. 1960;13(1):2-19. doi:10.14430/arctic3685

6. Lott DF. Sexual and Aggressive Behavior of Adult Male American Bison (*Bison bison*) in The Behaviour of Ungulates and its relation to management. *IUCN Publications new series*. 1974;I(24):382-394.

7. Lott DF. *American Bison, A Natural History*. University of California Press; 2002.

8. Harper JW, Maser JD. A macroscopic study of the brain of *Bison bison bison*, the American Plains Buffalo. *The Anatomical Record*. 1976;184(2):187-202. doi:10.1002/ar.1091840206

9. Budras K-D, Habel RE, Mülling CKW, Greenough PR, eds. *Bovine Anatomy*. Second. Schlütersche; 2011.

10. Liebich H-G, König HE. Axial Skeleton (skeleton axiale). In: König HE, Liebich H-G, eds. *Veterinary Anatomy of Domestic Mammals*. Sixth. Schattauer; 2014:53-116.

11. Matthews GE. Development of the Bovine Skull. 1972.

12. Soana S, Bertoni G, Gnudi G, Botti P. Osteogenesis of the Fetal Bovine Skull. Anatomia, Histologia, Embryologia. doi:10.1111/j.1439-0264.1996.tb00078.x

13. Farke AA. Evolution and functional morphology of the frontal sinuses in Bovidae (Mammalia: Artiodactyla), and implications for the evolution of cranial pneumaticity. *Zool J Linn Soc*. 2010;159(4):988-1014. doi:10.1111/j.1096-3642.2009.00586.x

14. Koyabu D, Maier W, Sánchez-Villagra MR. Paleontological and developmental evidence resolve the homology and dual embryonic origin of a mammalian skull bone, the interparietal. *PNAS*. 2012;109(35):14075-14080. doi:10.1073/pnas.1208693109

15. Martin RB, Boardman DL. The effects of collagen fiber orientation, porosity, density, and mineralization on bovine cortical bone bending properties. *Journal of Biomechanics*. 1993;26(9):1047-1054. doi:10.1016/S0021-9290(05)80004-1

16. Currey JD. The many adaptations of bone. *Journal of Biomechanics*. 2003;36(10):1487-1495. doi:10.1016/S0021-9290(03)00124-6

17. Locke M. Structure of long bones in mammals. *Journal of Morphology*. 2004;262(2):546-565. doi:10.1002/jmor.10282

18. Novitskaya E, Chen P-Y, Lee S, et al. Anisotropy in the compressive mechanical properties of bovine cortical bone and the mineral and protein constituents. *Acta Biomaterialia*. 2011;7(8):3170-3177. doi:10.1016/j.actbio.2011.04.025

19. Burr DB. Bone Morphology and Organization. In: Burr DB, Allen MR, eds. *Basic and Applied Bone Biology*. 2nd ed. Academic Press; 2019:3-26.

20. Thompson JC. *Netter's Concise Orthopaedic Anatomy*. Second. Elsevier; 2016.

21. Newman E, Turner AS, Wark JD. The potential of sheep for the study of osteopenia: Current status and comparison with other animal models. *Bone*. 1995;16(4, Supplement):S277-S284. doi:10.1016/S8756-3282(95)80121-9

22. Pearce AI, Richards RG, Milz S, Schneider E, Pearce SG. Animal models for implant biomaterial research in bone: a review. *Eur Cell Mater*. 2007;13:1-10.

23. Katz JL, Yoon HS. The structure and anisotropic mechanical properties of bone. *IEEE Trans Biomed Eng*. 1984;31(12):878-884. doi:10.1109/TBME.1984.325252

24. Keaveny TM, Morgan EF, Niebur GL, Yeh OC. Biomechanics of Trabecular Bone. *Annu Rev Biomed Eng*. 2001;3(1):307-333. doi:10.1146/annurev.bioeng.3.1.307

25. Carter DR, Hayes WC, Schurman DJ. Fatigue life of compact bone—II. Effects of microstructure and density. *Journal of Biomechanics*. 1976;9(4):211-218. doi:10.1016/0021-9290(76)90006-3

26. Manilay Z, Novitskaya E, Sadovnikov E, McKittrick J. A comparative study of young and mature bovine cortical bone. *Acta Biomaterialia*. 2013;9(2):5280-5288. doi:10.1016/j.actbio.2012.08.040

27. Grove C, Jerram DA. jPOR: An ImageJ macro to quantify total optical porosity from blue-stained thin sections. *Computers & Geosciences*. 2011;37(11):1850-1859. doi:10.1016/j.cageo.2011.03.002

28. Rasband WS. *ImageJ*. Bethesda, MD: U.S. National Institues of Health; 1997. https://imagej.nih.gov/ij/.

29. Currey J. Comparative Mechanical Properties and Histology of Bone. *Am Zool*. 1984;24(1):5-12. doi:10.1093/icb/24.1.5

30. Cow Compact Bone, Fibrolamellar. http://www.matweb.com/search/datasheet.aspx?MatGUID=e312f442ba2942e88ba30ec764d0ff8c. Accessed October 17, 2019.

CHAPTER III

MOLECULAR SYSTEMATICS OF *BISON* AND *BOS* (ARTIODACTYLA: BOVIDAE)

3.1 Introduction

In general, a lack information exists regarding the mechanical properties of North American bison (*Bison bison*) bone; however, the mechanical properties of domestic cow (*Bos taurus*) bone have been characterized,[1–4] and, due to cross-breeding, the histories of these two species in North America have been intertwined for over a century.[5]

Almost all extant North American plains bison (*Bison bison bison*) are descended from approximately 76-84 captured individuals maintained in five private herds established in the late nineteenth century or from a remnant population that still remained in Yellowstone National Park.[5–7] As these private herds were started with less than 100 wild-caught bison, extant *B. bison bison* are genetically bottlenecked.[5,7] In addition to bottlenecking, the genetics of North American bison have been further confounded by the cross-breeding of North American bison with domestic cattle.[5,8,9]

Domestic cattle mitochondrial DNA (mtDNA) has been recognized in several individual wild North American plains bison found in Custer State Park, South Dakota, the Maxwell and Finney State Game Refuges, Kansas, the National Bison Range, Montana, and Antelope Island State Park, Utah.[7,10,11] Further, domestic cattle mtDNA has also been recognized in private bison herds in Texas and Montana.[11,12] An argument exists that the domestic cattle mtDNA in these individuals originates from introgression between bison and domestic cattle within the founder herds.[10] Of the founder herds, three of the five were known to contain hybrids, and the fate of these hybrids is largely undocumented.[6] Within Bovidae, introgression among species is not uncommon. For example, European bison (*Bison bonasus*) have been cross-bred with both North

American bison and domestic cattle,[13–15] the domestic yak (*Bos grunniens*) has been cross-bred with domestic cattle, [16,17] and zebu (*Bos indicus*) have also been cross-bred with domestic cattle.[18] The ability of various species within *Bison* and *Bos* to hybridize suggests that a low level of divergence exists between the genera which could result in inconclusive phylogenies.

Previous phylogenetic studies of bovines have found incongruent results when comparing phylogenies inferred from nuclear genes to those inferred from mitochondrial genes. For example, in nuclear gene based phylogenies, North American bison are recovered as sister to European bison, but in mitochondrial gene based phylogenies, the North American bison is recovered as sister to yaks.[12–14,19–21] Many of these phylogenies were inferred from individual nuclear or mitochondrial genes, or from concatenated or partitioned datasets, which can give conflicting results due to a general lack of robustness when using individual genes or from incomplete lineage sorting of the chosen gene.[14,15,22] Additionally, nuclear DNA is bi-parentally inherited while mtDNA is only inherited through the maternal lineage; therefore, the effective population size is increased when using nuclear genes. The possibility exists that a retained ancestral polymorphism is present in bovines leading to incomplete lineage sorting, that, when coupled with introgression (horizontal gene transfer) and domestication, obscures the true phylogentic relationships within the group resulting in the incongruent nuclear and mtDNA phylogenies.[23–27]

To overcome the limitations of using single, concatenated, or partitioned gene datasets to infer phylogenetic relationships, unpartitioned sequences for the complete mitochondrial genome (mitogenome) for four taxa of *Bison* and and seven taxa of *Bos* were used to infer their relationships and genetic distances. It is expected that use of the mitogenome for phylogentic analysis will provide increased resolution over single or concatenated gene datasets.[28–30] Further,

this analysis includes sequences for three extinct species – the steppe bison (*Bison priscus*), the woodland bison (*Bison schoetensacki*), and the auroch (*Bos primigenius*) which should help further elucidate the relationships between *Bison* and *Bos*.

3.2 Materials and Methods

To ascertain the phylogenetic relationships and genetic distances between *Bison* and *Bos*, sequences of the ~16,340 base pair complete mitochondrial genome from species across each genus plus one root species were selected from GenBank. Shotgun, predicted, and heavily wobbled sequences were excluded from analyses with the exception of the single Hereford sequence which was a shotgun assembly. Additionally, sequences for *Bos taurus* were restricted to those breeds common in North America due to their potential for introgression with North American bison[11,32] resulting in a dataset containing 41 complete mitogenome sequences (Tables 3.1 and 3.2). Of note, sequences of the kouprey (*Bos sauveli*) mitochondrial genome are currently unavailable. Further, the kouprey is listed as critically endangered, but may already be extinct.[31]

A complete alignment of the mitogenome sequences was performed using the multiple alignment mode available in ClustalX,[33] and the subsequent alignment was verified by eye. Due to the number of both sequences and characters, WinClada v. 1.00.08[34] was used to perform a tree bi-section reconnection (TBR) parsimony ratchet[35] with 200 iterations per repetition, 1 tree to hold, and 1,747 characters to sample. A heuristic search of the tree space returned from the ratchet was then performed using the unconstrained mutltiple TBR option with 5000 maximum trees to keep, 500 replications, and 5 starting trees per each replication. Bootstrap replicates were set a 1000, with 10 search repititions per replicate, and 2 starting trees per repetition. Trees were rooted with the Eland antelope (*Tragelaphus oryx*), a distant relative to both genera.[36] Following

the phylogenetic analysis, both the uncorrected pairwise *p*-distances and the Tamura-Nei genetic distances were calculated using the transistions + tranversions option using MEGA (Molecular Evolutionary Genetics Analysis) version X to estimate the sequence divergence between groups.[37]

When calculating the uncorrected pairwise *p*-distance, p represents the proportion of nucleotide sites that differ between two sequences (Eq. 3.1).[37] An increase in the *p*-distance implies a concomitant increase in the level of divergence between the compared sequences.

$$p = \frac{n_d}{L} \tag{3.1}$$

where:

n_d = the number of nucleotides that differ between two sequences

L = the lengths of the two compared sequences

The uncorrected pairwise *p*-distance does not correct for the same sites with multiple substitutions, for variability in transitional and transversional rate, or for evolutionary rate variability among sites;[37] therefore, the uncorrected *p*-distances were compared with the distances obtained from the Tamura-Nei distance model which takes into account subustitution rates across different sites and variability in the transitional and tranversional rates (Eqs. 3.2-3.8).[37,38]

$$d = -k_1 log_e(w_1) - k_2 log_e(w_2) - k_3 log_e(w_3) \tag{3.2}$$

$$k_1 = \frac{2g_A g_G}{g_R} \tag{3.3}$$

$$k_2 = \frac{2g_T g_C}{g_Y} \tag{3.4}$$

$$k_3 = 2\left(g_R g_Y - \frac{g_A g_G g_Y}{g_R} - \frac{g_T g_C g_R}{g_Y}\right) \tag{3.5}$$

$$w_1 = 1 - \frac{P_1}{k_1} - \frac{Q}{2g_R} \tag{3.6}$$

$$w_2 = 1 - \frac{P_2}{k_2} - \frac{Q}{2g_Y} \quad (3.7)$$

$$w_3 = 1 - \frac{Q}{2g_R g_Y} \quad (3.8)$$

where:

g_A = frequency of adenine (A)

g_C = frequency of cytosine (C)

g_G = frequency of guanine (G)

g_T = frequency of thymine (T)

$g_R = g_A + g_G$

$g_Y = g_T + g_C$

P_1 = transitions between purines (A and G)

P_2 = transitions between pyrimidines (C and T)

Q = transversions (purine to pyrimidine or pyrimidine to purine)

3.3 Results

3.3.1 Phylogenetic Systematics

The aligned dataset consited of 17,476 characters, 15,330 of which were non-parsimony informative (NPI) leaving 2,146 parsimony informative (PI) characters. Nineteen trees with a length (L) of 4,946 were returned from the parsimony ratchet. The heuristic search of the parsimony ratchet tree space returned 118 trees all with an L of 4946. Eleven nodes were collapsed on the strict-consensus tree (Fig. 3.1).

Based on the inferred topology, a monophyletic clade containing the gaur (*Bos gaurus*) and gayal (*Bos frontalis*) is sister to both the *Bison* and *Bos* genera. Both *Bison* and *Bos* are paraphyletic, yet fall into one of two larger biogeographic clades, either the Beringian-American

clade or the Indo-European clade. The Beringian-American clade contains the extinct steppe bison (*Bison priscus*), North American plains and wood bison (*Bison bison bison* and *Bison bison athabascae*, respectively) and both the wild and domesticated yak (*Bos mutus* and *Bos grunniens*, respectively). Within the Beringian-American clade, a well-supported monophyletic yak clade is recovered as sister the extinct steppe bison. In another well-supported relationship, the steppe bison is recovered as sister to all extant North American bison. Within the North American bison clade, no strongly supported geographic or subspecies structuring is noted.

Recovery of the Beringian-American clade as sister to the Indo-European clade is well-supported. Within the Indo-European clade, a monophyletic bison clade containing the European bison (*Bison bonasus*) and the extinct woodland bison (*Bison schoetensacki*) is recovered as sister to the extinct auroch (*Bos primigenius*), the zebu (*Bos indicus*), domestic cattle (*Bos taurus*), the banteng (*Bos javanicus*) and hybrids (North American bison that contain domestic cattle mtDNA). In well-supported relationships, the zebu is recovered as being sister to the auroch, domestic cattle, the banteng, and the hybrids, while the auroch is recovered as sister to all domestic cattle, the banteng, and the hybrids. Domestic cattle are collapsed into a polytomy that is recovered as sister to the banteng and the hybrids. The hybrids exhibit poorly supported structuring; therefore, little resolution exists between domestic cattle breeds and the hybrids.

3.3.2 Genetic Distances

Based on the mitogenome sequences, divergence both within and between *Bison* and *Bos* is low, and the distances recovered by the uncorrected pairwise *p*-distance and the Tamura-Nei model are similar (Tables 3.3 and 3.4). An approximately 6.0% divergence between the Beringian-American and Indo-European clades is recovered by both models. Intergroup

divergence for all groups was recovered as 0.0% by both models, with the exception of the yak group, for which both models estimated a distance of 1.0%.

Within *Bos*, the maximum divergence (6.4 – 6.8%) occurs between the gaur and the banteng, and the minimum divergence (<1.0%) occurs between domestic cattle and the banteng. The maximum divergence within the genus *Bison* (6.1 – 6.5%) occurs between the North American bison and the European bison while the minimum divergence (<1.0%) occurs between the steppe bison and the North American bison (Tables 3.3 and 3.4).

Among species known to hybridize, the estimated genetic divergence between North American bison and domestic cattle is approximately 5.9-6.3%, and the estimated divergence between North American bison and European bison is approximately 6.1-6.5%. An estimate of 5.3-5.6% divergence is recovered between the European bison and domestic cattle. Similar to the North American and European bison, a 6.1-6.5% divergence is recovered between the domestic yak and domestic cattle. Finally, zebu and domestic cattle have been cross-bred, and their estimated divergence is 1.5% (Tables 3.3 and 3.4).

3.4 Discussion and Conclusions

The results of the phylogenetic analysis largely concur with the findings of previous phylogenetic analyses of *Bison* and *Bos* using mitochondrial genes. As expected, North American bison are recovered as sister to wild and domestic yak, the steppe bison is recovered as sister to all North American bison, the woodland bison is recovered as sister to the European bison, and the gaur and gayal are recovered as sister to yak, bison, and cattle.[12,14,39–41]

Addition of the mitogenomes of the extinct species to the analysis suggests that a biogeographic sorting is responsible for the overall structure of the tree. Ancestral bison are believed to have originated India and China before spreading into Europe and eventually North

America.[39] The steppe bison once ranged throughout Europe, Russia, and eventually reached North America via Beringia some 130,000-75,000 years ago before its extinction approximately 10,000 years ago.[39,40] Evidence from the phylogenetic analysis suggests that the North American bison may be the direct descendent of the steppe bison.

Similar to ancestral bison, the gaur ranges from India to China and throughout eastern Asia, while the wild and domestic yaks are distributed from India to Russia.[17,42] Not only do the ranges of the gaur, yak, and steppe bison overlap, evidence from mutations in mtDNA also suggests that introgression occurred between the bison and the yak approximately 700,000 years ago[21] explaining the recovery of yaks as sister to the steppe bison. The recovery of the gaur and gayal as sister to *Bison* and *Bos* is unclear and may be the result of a historical introgression,[43] but further research into the gaur and gayal genomes is needed. Each of these taxa which currently range from Asia to North America form the Beringian-American clade which is recovered as sister to an Indo-European clade.

The Indo-European clade consists of the European bison, the extinct woodland bison, the extinct auroch, the banteng, and both zebuine and taurine cattle (*Bos indicus* and *Bos taurus*, respectively). Additionally, North American bison that contain domestic cattle mtDNA are also recovered within this clade.

Similar to the steppe bison, the woodland bison ranged from Europe into Asia, but apparently never crossed Beringia into North America perhaps due to habitat differences. The woodland bison and the steppe bison are believed to have occupied different niches, with the woodland bison preferring forested habitats, and the steppe bison preferring open grasslands.[14,39] Due to climate, Beringia is believed to have been covered by a tundra biome with little opportunity for forestation[44] preventing the dispersal of woodland bison into North America.

Because of the ranges of the steppe and woodland bison, confusion has existed regarding which was the closest relative of the European bison.[14,39]

Currently, the European bison is found in Europe and Caucasus. Recent analyses of mtDNA have recovered the woodland bison as the ancestor to the European bison, and like its ancestor, the European bison inhabits forested habitats.[14,45] These findings suggest that the paraphyly of *Bison* is driven not only by biogeography, but also by differences in habitat usage.

The extinct auroch, which ranged throughout Europe, Asia, Africa, and India is considered to be the wild ancestor to both zebuine and taurine cattle. Taurine cattle are generally considered European breeds while zebuine cattle are considered Asian breeds.[18] While the auroch is recovered as the sister to taurine cattle and the banteng, zebuine cattle are recovered as basal to the auroch, taurine cattle, and the banteng. Recovery of the banteng as sister to taurine cattle and the hybrids was unexpected. Previous phylogenies have recovered the banteng as sister to the gaur.[41,46] The recovery of the banteng as sister to the gaur may be an artifact of incomplete lineage sorting; whereas, recovery of the banteng as sister to domestic cattle may be the result of introgression. Introgression between the banteng and cattle has been documented which may explain the placement of the banteng amongst the cattle.[47,48] It is also possible that a historical migration and isolation of either aurochs or taurine cattle into southeastern Asia resulted in the evolution of the banteng.[49] Similar to the gaur and gayal, further research regarding the banteng genome is needed to determine its evolutionary history. Placement of the banteng may also be complicated due to the complex relationship between the auroch and cattle resulting from both introgression between aurochs and cattle as well as multiple domestication events.[18]

Biogeographic structuring is evident when considering the two large clades recovered. Further, *Bison* not only exhibits biogeographical structuring, but also ecological structuring.

Such structuring suggests that although species of *Bison* and *Bos* are not necessarily endemic, natural gene flow within each genus or between the genera in Europe, Asia, and North America has been restricted for some time. Despite the biogeographical structuring, the overall sequence divergence is low and facilitates hybridization among species.

While hybridization may result in speciation events and confer beneficial genes to subsequent generations, the opposite effect is also possible. Transfer of deleterious genes via hybridization can decrease the overall fitness of a species through functional changes or due to increased susceptibility to disease.[12] When coupled with the relatively recent bottleneck of North American bison, hybridization of North American bison with domestic cattle, while producing traits beneficial to humans, could potentially result in irreparable damage that again places the North American bison on the brink of extinction through decreased fitness or through absorption of the cattle genome into that of bison. Regarding the fate of North American bison, Lott [5] has stated, "the most vivid threat today is eradication by modification." For the conservation of not only North American bison, but also the other species of *Bison* and *Bos* to be successful, an understanding of their phylogenetic histories and the effects of hybridization on the fitness of species must be taken into account. Despite the complicated phylogenetic tree, however, genetic divergence between *Bison bison* and *Bos taurus* is low, suggesting that the material properties of domestic cattle bone are a suitable proxy for those of bison bone.

Table 3.1

Complete Mitochondrial Genome Sequences of Bison Used in the Phylogenetic Analyses

GenBank Accession Number	Species	Common Name	Reference
JN632704.1	*Tragelaphus oryx*	Common Eland Antelope[a]	Hassanin *et al.*[50]
KM593920.1	*Bison priscus*	Steppe Bison[b]	Marsolier-Kergoat *et al.*[39]
NC_027233.1	*Bison priscus*	Steppe Bison[b]	Marsolier-Kergoat *et al.*[39]
GU947005.1	*Bison bison athabascae*	North American Wood Bison	Douglas *et al.*[12]
GU947006.1	*Bison bison athabascae*	North American Wood Bison	Douglas *et al.*[12]
GU947002.1	*Bison bison bison*	North American Plains Bison[c]	Douglas *et al.*[12]
GU946979.1	*Bison bison bison*	North American Plains Bison[d]	Douglas *et al.*[12]
GU946976.1	*Bison bison bison*	North American Plains Bison[d]	Douglas *et al.*[12]
GU947004.1	*Bison bison bison*	North American Plains Bison[e]	Douglas *et al.*[12]
GU946978.1	*Bison bison bison*	North American Plains Bison[d]	Douglas *et al.*[12]
GU947001.1	*Bison bison bison*	North American Plains Bison[f]	Douglas *et al.*[12]
GU947000.1	*Bison bison bison*	North American Plains Bison[g]	Douglas *et al.*[12]
GU947011.1	Hybrid	North American Bison with Domestic Cow mtDNA	Douglas *et al.*[12]
GU947013.1	Hybrid	North American Bison with Domestic Cow mtDNA	Douglas *et al.*[12]
GU947007.1	Hybrid	North American Bison with Domestic Cow mtDNA	Douglas *et al.*[12]
GU947015.1	Hybrid	North American Bison with Domestic Cow mtDNA	Douglas *et al.*[12]
GU947009.1	Hybrid	North American Bison with Domestic Cow mtDNA	Douglas *et al.*[12]
HQ223450.1	*Bison bonasus*	European Bison or Wisent	Unpublished
NC_014044.1	*Bison bonasus*	European Bison or Wisent	Zeyland *et al.*[21]
NC_033873.1	*Bison schoetensacki*	Woodland Bison[b]	Palacio *et al.*[14]
KU886087.1	*Bison schoetensacki*	Woodland Bison[b]	Palacio *et al.*[14]

a. Outgroup; b. Extinct; c. Texas State Bison Herd; d. Private Bison Herd, Montana; e. Yellowstone National Park, Wyoming; f. National Bison Range, Montana;

g. Fort Niobrara National Wildlife Refuge, Nebraska

Table 3.2
Complete Mitochondrial Genome Sequences of *Bos* Used in the Phylogenetic Analyses

GenBank Accession Number	Species	Common Name	Reference
AY676872.1	*Bos taurus* (Angus Breed)	Domestic Cow	Unpublished
AY676869.1	*Bos taurus* (Angus Breed)	Domestic Cow	Unpublished
AY676865.1	*Bos taurus* (Angus Breed)	Domestic Cow	Unpublished
AY676871.1	*Bos taurus* (Angus Breed)	Domestic Cow	Unpublished
AY676867.1	*Bos taurus* (Angus Breed)	Domestic Cow	Unpublished
GU947021.1	*Bos taurus* (Longhorn Breed)	Domestic Cow	Douglas *et al.*[12]
CM008198.1	*Bos taurus* (Hereford Breed)	Domestic Cow	Unpublished
GU985279.1	*Bos primigenius*	Auroch[b]	Edwards *et al.*[51]
NC_013996.1	*Bos primigenius*	Auroch[b]	Edwards *et al.*[51]
JQ437479.1	*Bos primigenius*	Auroch[b]	Unpublished
NC_025563.1	*Bos mutus*	Wild Yak	Na *et al.*[16]
KM233417.1	*Bos mutus*	Wild Yak	Na *et al.*[16]
AY684273.2	*Bos grunniens*	Domestic Yak	Gu *et al.*[52]
KM233416.1	*Bos grunniens*	Domestic Yak	Guangxin *et al.*[53]
AF492350.1	*Bos indicus*	Zebu	Hiendleder *et al.*[18]
NC_005971.1	*Bos indicus*	Zebu	Unpublished
NC_024818.1	*Bos gaurus*	Gaur	Hassanin *et al.*[50]
JN632604.1	*Bos gaurus*	Gaur	Hassanin *et al.*[50]
NC_036020.1	*Bos frontalis*	Gayal or Mithun	Unpublished
MF614103.1	*Bos frontalis*	Gayal or Mithun	Unpublished
FJ997262.1	*Bos javanicus*	Banteng	Unpublished
NC_012706.1	*Bos javanicus*	Banteng	Unpublished

b. Extinct

Table 3.3
Intergroup Divergence Estimates Based on Uncorrected Pairwise *p*-Distances

	Outgroup	Steppe Bison	North American Bison	Yak	Domestic Cattle	Hybrid	Auroch	European Bison	Zebu	Woodland Bison	Gaur	Banteng
Outgroup												
Steppe Bison	0.13276											
North American Bison	0.13298	0.00693										
Yak	0.13379	0.02616	0.02815									
Domestic Cattle	0.13350	0.05877	0.05910	0.06086								
Hybrid	0.13375	0.05887	0.05905	0.06100	0.00107							
Auroch	0.13348	0.05783	0.05874	0.06024	0.00429	0.00430						
European Bison	0.13382	0.06009	0.06115	0.06060	0.05280	0.05299	0.05252					
Zebu	0.13380	0.05770	0.05863	0.05926	0.01466	0.01484	0.01420	0.05337				
Woodland Bison	0.13269	0.05954	0.06085	0.06008	0.05204	0.05217	0.05180	0.02065	0.05188			
Gaur	0.13294	0.05461	0.05634	0.05730	0.06394	0.06393	0.06387	0.06430	0.06353	0.06179		
Banteng	0.13347	0.05891	0.05919	0.06100	0.00098	0.00107	0.00424	0.05300	0.01479	0.05226	0.06397	
Gayal	0.13236	0.05517	0.05674	0.05709	0.06358	0.06358	0.06376	0.06453	0.06365	0.06263	0.00275	0.06347

Table 3.4
Intergroup Divergence Estimates Based on the Tamura-Nei Distance Model

	Outgroup	Steppe Bison	North American Bison	Yak	Domestic Cattle	Hybrid	Auroch	European Bison	Zebu	Woodland Bison	Gaur	Banteng
Outgroup												
Steppe Bison	0.15327											
North American Bison	0.15355	0.00699										
Yak	0.15501	0.02691	0.02902									
Domestic Cattle	0.15392	0.06264	0.06302	0.06509								
Hybrid	0.15421	0.06276	0.06296	0.06525	0.00108							
Auroch	0.15386	0.06159	0.06263	0.06441	0.00431	0.00432						
European Bison	0.15485	0.06425	0.06549	0.06486	0.05596	0.05616	0.05565					
Zebu	0.15423	0.06143	0.06248	0.06327	0.01488	0.01507	0.01442	0.05660				
Woodland Bison	0.15309	0.06359	0.06510	0.06424	0.05507	0.05520	0.05482	0.02112	0.05491			
Gaur	0.15289	0.05798	0.05998	0.06110	0.06863	0.06861	0.06855	0.06906	0.06811	0.06614		
Banteng	0.15386	0.06280	0.06311	0.06525	0.00098	0.00107	0.00426	0.05619	0.01502	0.05532	0.06865	
Gayal	0.15226	0.05859	0.06039	0.06082	0.06822	0.06821	0.06844	0.06928	0.06826	0.06709	0.00276	0.06808

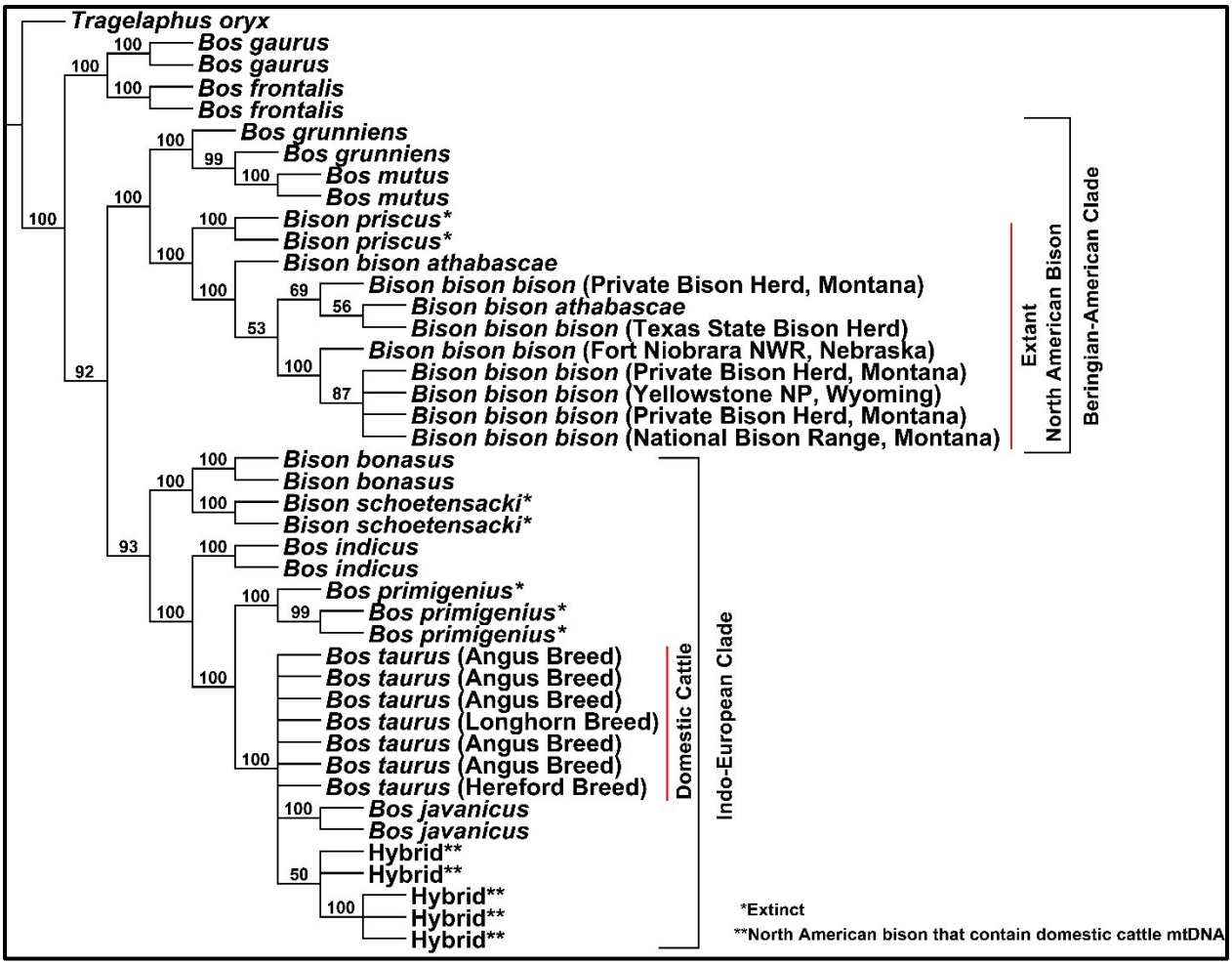

Figure 3.1 Complete mitochondrial genome strict-consensus topology (L = 4,893). Bootstrap support values are given above the branches.

References

1. Carter DR, Hayes WC, Schurman DJ. Fatigue life of compact bone—II. Effects of microstructure and density. *Journal of Biomechanics*. 1976;9(4):211-218. doi:10.1016/0021-9290(76)90006-3

2. Martin RB, Boardman DL. The effects of collagen fiber orientation, porosity, density, and mineralization on bovine cortical bone bending properties. *Journal of Biomechanics*. 1993;26(9):1047-1054. doi:10.1016/S0021-9290(05)80004-1

3. Novitskaya E, Chen P-Y, Lee S, et al. Anisotropy in the compressive mechanical properties of bovine cortical bone and the mineral and protein constituents. *Acta Biomaterialia*. 2011;7(8):3170-3177. doi:10.1016/j.actbio.2011.04.025

4. Manilay Z, Novitskaya E, Sadovnikov E, McKittrick J. A comparative study of young and mature bovine cortical bone. *Acta Biomaterialia*. 2013;9(2):5280-5288. doi:10.1016/j.actbio.2012.08.040

5. Lott DF. *American Bison, A Natural History*. University of California Press; 2002.

6. Coder GD. The National Movement to Preserve the American Buffalo in the United States and Canada Between 1880 and 1920. 1975. https://search.proquest.com/pqdtglobal/docview/302745670/citation/27267829C4A14724PQ/1. Accessed July 4, 2019.

7. Hedrick PW. Conservation genetics and North American bison (*Bison bison*). *J Hered*. 2009;100(4):411-420. doi:10.1093/jhered/esp024

8. Isenberg AC. *The Destruction of the Bison, An Environmental History, 1750-1920*. Cambridge University Press; 2000.

9. Canadian Wildlife Service, Committee on the Status of Endangered Wildlife in Canada. *COSEWIC Assessment and Status Report on the Plains Bison (*Bison Bison Bison*) and the Wood Bison (*Bison Bison Athabascae*) in Canada.*; 2013. https://central.bac-lac.gc.ca/.item?id=CW69-14-379-2014-eng&op=pdf&app=Library. Accessed July 5, 2019.

10. Polziehn RO, Strobeck C, Sheraton J, Beech R. Bovine mtDNA Discovered in North American Bison Populations. *Conservation Biology*. 1995;9(6):1638-1638. doi:10.1046/j.1523-1739.1995.09061638.x

11. Ward TJ, Bielawski JP, Davis SK, Templeton JW, Derr JN. Identification of domestic cattle hybrids in wild cattle and bison species: a general approach using mtDNA markers and the parametric bootstrap. *Animal Conservation*. 1999;2(1):51-57. doi:10.1111/j.1469-1795.1999.tb00048.x

12. Douglas KC, Halbert ND, Kolenda C, Childers C, Hunter DL, Derr JN. Complete mitochondrial DNA sequence analysis of *Bison bison* and bison-cattle hybrids: function and phylogeny. *Mitochondrion*. 2011;11(1):166-175. doi:10.1016/j.mito.2010.09.005

13. Verkaar ELC, Nijman IJ, Beeke M, Hanekamp E, Lenstra JA. Maternal and paternal lineages in cross-breeding bovine species. Has wisent a hybrid origin? *Mol Biol Evol*. 2004;21(7):1165-1170. doi:10.1093/molbev/msh064

14. Palacio P, Berthonaud V, Guérin C, et al. Genome data on the extinct Bison schoetensacki establish it as a sister species of the extant European bison (*Bison bonasus*). *BMC Evolutionary Biology*. 2017;17(1):48. doi:10.1186/s12862-017-0894-2

15. Wang K, Lenstra JA, Liu L, et al. Incomplete lineage sorting rather than hybridization explains the inconsistent phylogeny of the wisent. *Communications Biology*. 2018;1(1):169. doi:10.1038/s42003-018-0176-6

16. Na R-S, Zhao Y-J, Gao H-J, An T-W, Huang Y-F, E G-X. Complete mitochondrial genome of the Yakow (*Bos primigenius taurus* × *Bos grunniens*) in China. *Mitochondrial DNA A DNA Mapp Seq Anal*. 2016;27(6):3826-3827. doi:10.3109/19401736.2014.953134

17. Qi XB, Jianlin H, Wang G, Rege JEO, Hanotte O. Assessment of cattle genetic introgression into domestic yak populations using mitochondrial and microsatellite DNA markers. *Animal Genetics*. 2010;41(3):242-252. doi:10.1111/j.1365-2052.2009.01989.x

18. Hiendleder S, Lewalski H, Janke A. Complete mitochondrial genomes of *Bos taurus* and *Bos indicus* provide new insights into intra-species variation, taxonomy and domestication. *Cytogenet Genome Res*. 2008;120(1-2):150-156. doi:10.1159/000118756

19. Nijman IJ, Boxtel DCJV, Cann LMV, Marnoch Y, Cuppen E, Lenstra JA. Phylogeny of Y chromosomes from bovine species. *Cladistics*. 2008;24(5):723-726. doi:10.1111/j.1096-0031.2008.00201.x

20. Hassanin A, An J, Ropiquet A, Nguyen TT, Couloux A. Combining multiple autosomal introns for studying shallow phylogeny and taxonomy of Laurasiatherian mammals: Application to the tribe Bovini (Cetartiodactyla, Bovidae). *Mol Phylogenet Evol*. 2013;66(3):766-775. doi:10.1016/j.ympev.2012.11.003

21. Zeyland J, Wolko L, Lipiński D, et al. Tracking of wisent-bison-yak mitochondrial evolution. *J Appl Genet*. 2012;53(3):317-322. doi:10.1007/s13353-012-0090-4

22. Ponce de León FA, Liu W. Bovine X and Y Chromosomes. In: Womack JE, ed. *Bovine Genomics*. First. John Wiley & Sons, Inc.; 2012.

23. Maddison WP. Gene Trees in Species Trees. *Syst Biol*. 1997;46(3):523-536. doi:10.1093/sysbio/46.3.523

24. Charlesworth B, Bartolomé C, Noël V. The detection of shared and ancestral polymorphisms. *Genetics Research*. 2005;86(2):149-157. doi:10.1017/S0016672305007743

25. Steiner CC, Mitelberg A, Tursi R, Ryder OA. Molecular phylogeny of extant equids and effects of ancestral polymorphism in resolving species-level phylogenies. *Molecular Phylogenetics and Evolution*. 2012;65(2):573-581. doi:10.1016/j.ympev.2012.07.010

26. Sousa V, Hey J. Understanding the Origin of Species with Genome-Scale Data: the Role of Gene Flow. *Nat Rev Genet*. 2013;14(6):404-414. doi:10.1038/nrg3446

27. Zhou Y, Duvaux L, Ren G, Zhang L, Savolainen O, Liu J. Importance of incomplete lineage sorting and introgression in the origin of shared genetic variation between two closely related pines with overlapping distributions. *Heredity (Edinb)*. 2017;118(3):211-220. doi:10.1038/hdy.2016.72

28. Boore JL, Macey JR, Medina M. Sequencing and comparing whole mitochondrial genomes of animals. *Meth Enzymol*. 2005;395:311-348. doi:10.1016/S0076-6879(05)95019-2

29. Yu L, Li Y-W, Ryder OA, Zhang Y-P. Analysis of complete mitochondrial genome sequences increases phylogenetic resolution of bears (Ursidae), a mammalian family that experienced rapid speciation. *BMC Evol Biol*. 2007;7:198. doi:10.1186/1471-2148-7-198

30. Duchêne S, Archer FI, Vilstrup J, Caballero S, Morin PA. Mitogenome Phylogenetics: The Impact of Using Single Regions and Partitioning Schemes on Topology, Substitution Rate and Divergence Time Estimation. *PLoS One*. 2011;6(11). doi:10.1371/journal.pone.0027138

31. Timmins RJ, Burton J, Hedges S. *Bos sauveli*. The IUCN Red List of Threatened Species 2016. *eT2890A46363360*. 2016. http://dx.doi.org/10.2305/IUCN.UK.2016-2.RLTS.T2890A46363360.en.

32. Halbert ND, Ward TJ, Schnabel RD, Taylor JF, Derr JN. Conservation genomics: disequilibrium mapping of domestic cattle chromosomal segments in North American bison populations. *Molecular Ecology*. 2005;14(8):2343-2362. doi:10.1111/j.1365-294x.2005.02591.x

33. Thompson JD, Gibson TJ, Plewniak F, Jeanmougin F, Higgins DJ. The ClustalX windows interface: flexible strategies for multiple sequence alignment aided by quality analysis tools. *Nucleic Acids Research*. 1997;25:4876-4882.

34. Nixon K. *Winclada*.; 2002. http://www.diversityoflife.org/winclada/.

35. Nixon KC. The Parsimony Ratchet, a New Method for Rapid Parsimony Analysis. *Cladistics*. 1999;15(4):407-414. doi:10.1111/j.1096-0031.1999.tb00277.x

36. Bibi F. A multi-calibrated mitochondrial phylogeny of extant Bovidae (Artiodactyla, Ruminantia) and the importance of the fossil record to systematics. *BMC Evol Biol*. 2013;13:166. doi:10.1186/1471-2148-13-166

37. Kumar S, Stecher G, Li M, Knyaz C, Tamura K. MEGA X: Molecular Evolutionary Genetics Analysis across computing platforms. *Molecular Biology and Evolution*. 2018;35:1547-1549.

38. Tamura K, Nei M. Estimation of the number of nucleotide substitutions in the control region of mitochondrial DNA in humans and chimpanzees. *Mol Biol Evol*. 1993;10(3):512-526. doi:10.1093/oxfordjournals.molbev.a040023

39. Marsolier-Kergoat M-C, Palacio P, Berthonaud V, et al. Hunting the Extinct Steppe Bison (*Bison priscus*) Mitochondrial Genome in the Trois-Frères Paleolithic Painted Cave. *PLoS ONE*. 2015;10(6):e0128267. doi:10.1371/journal.pone.0128267

40. Shapiro B, Drummond AJ, Rambaut A, et al. Rise and Fall of the Beringian Steppe Bison. *Science*. 2004;306(5701):1561-1565. doi:10.1126/science.1101074

41. Hassanin A, Ropiquet A. Molecular phylogeny of the tribe Bovini (Bovidae, Bovinae) and the taxonomic status of the Kouprey, Bos sauveli Urbain 1937. *Molecular Phylogenetics and Evolution*. 2004;33(3):896-907. doi:10.1016/j.ympev.2004.08.009

42. Choudhury A. Distribution and conservation of the Gaur *Bos gaurus* in the Indian Subcontinent. *Mammal Review*. 2002;32(3):199-226. doi:10.1046/j.1365-2907.2002.00107.x

43. Wu D-D, Ding X-D, Wang S, et al. Pervasive introgression facilitated domestication and adaptation in the *Bos* species complex. *Nature Ecology & Evolution*. 2018;2(7):1139. doi:10.1038/s41559-018-0562-y

44. Hoffecker JF, Elias SA, O'Rourke DH. Out of Beringia? *Science*. 2014;343(6174):979-980. doi:10.1126/science.1250768

45. Kuemmerle T, Radeloff VC, Perzanowski K, et al. Predicting potential European bison habitat across its former range. *Ecological Applications*. 2011;21(3):830-843. doi:10.1890/10-0073.1

46. Price SA, Bininda-Emonds ORP, Gittleman JL. A complete phylogeny of the whales, dolphins and even-toed hoofed mammals (Cetartiodactyla). *Biol Rev Camb Philos Soc*. 2005;80(3):445-473.

47. Nijman IJ, Otsen M, Verkaar ELC, et al. Hybridization of banteng (*Bos javanicus*) and zebu (*Bos indicus*) revealed by mitochondrial DNA, satellite DNA, AFLP and microsatellites. *Heredity*. 2003;90(1):10. doi:10.1038/sj.hdy.6800174

48. Davis SK, Read B, Balke J. Protein electrophoresis as a management tool: Detection of hybridization between banteng (*Bos javanicus* d'Alton) and domestic cattle. *Zoo Biology*. 1988;7(2):155-164. doi:10.1002/zoo.1430070209

49. Ajmone-Marsan P, Garcia JF, Lenstra JA. On the origin of cattle: How aurochs became cattle and colonized the world. *Evolutionary Anthropology: Issues, News, and Reviews*. 2010;19(4):148-157. doi:10.1002/evan.20267

50. Hassanin A, Delsuc F, Ropiquet A, et al. Pattern and timing of diversification of Cetartiodactyla (Mammalia, Laurasiatheria), as revealed by a comprehensive analysis of mitochondrial genomes. *C R Biol*. 2012;335(1):32-50. doi:10.1016/j.crvi.2011.11.002

51. Edwards CJ, Magee DA, Park SDE, et al. A complete mitochondrial genome sequence from a mesolithic wild aurochs (*Bos primigenius*). *PLoS ONE*. 2010;5(2):e9255. doi:10.1371/journal.pone.0009255

52. Gu Z, Zhao X, Li N, Wu C. Complete sequence of the yak (*Bos grunniens*) mitochondrial genome and its evolutionary relationship with other ruminants. *Mol Phylogenet Evol*. 2007;42(1):248-255. doi:10.1016/j.ympev.2006.06.021

53. Guangxin E, Na R-S, Zhao Y-J, Gao H-J, An T-W, Huang Y-F. Complete mitochondrial genome of the a rare subspecies of genus Bos, Tianzhu white yak from Tibetan area in China. *Mitochondrial DNA A DNA Mapp Seq Anal*. 2016;27(2):1443-1444. doi:10.3109/19401736.2014.953084

CHAPTER IV

FINITE ELEMENT ANALYSIS (FEA) OF THE MECHANISMS OF IMPACT MITIGATION INHERENT TO THE NORTH AMERICAN BISON (*BISON BISON*) SKULL

4.1 Introduction

North American bison (Bovidae: *Bison bison bison* and Bovidae: *Bison bison athabascae*) bulls engage in threatening and fighting behaviors to both assert their dominance and to win the right to mate with a bison cow. These behaviors are exemplified during the rut (mating season), and begin with threatening behaviors that include the bulls urinating and then wallowing in the urine, bellowing, snorting, and posturing.[1–4] Posturing behaviors include approaching one another with a hesitant gait and engaging in either a head-on threat, a nod-threat, or a broadside-threat.[1–3] The head-on threat resembles a charge, but typically occurs at a slow walk and ends with the aggressor raising his head and stopping short of his opponent. During a nod-threat, the bulls move close to one another, with their heads held at one side. The bulls will then simultaneously raise and lower their heads in a nodding motion. A broadside-threat involves mostly posturing. The aggressor stands at a distance from his opponent bellowing while holding his body stiff in a straight line. During a broadside-threat, the bulls may be facing one another or parallel to one another, but their heads are not moved to one side as in the nod-threat [3,4]. If neither bull submits to the threats, then fighting behaviors ensue.[1,3,4]

Fighting begins either with one bull slowly approaching the other, with one bull shaking his head at the other, or with one bull charging the other.[1–4] While the bulls may attempt to use their horns to gore the flank of their opponents, the main fighting mechanism consists of head-to-head ramming about the caudal frontal and interparietal bones followed by head-to-head shoving (Fig.1.1); whereby, the dominant bull may push his challenger backwards by several feet, and in some cases, cause the challenger to be flipped onto his back.[1–4] The fighting ends when one bull submits to the other by backing, turning, or running away, or by the resumption of grazing. Typically, the fights do not result in death; however, goring injuries may become infected and ultimately lead to the death of a bull.[1,4]

Although the threatening and fighting behaviors are well documented, little is known of how the cranial anatomy protects the bison during head-to-head collisions. Bison bulls may range in mass from ~492 kilograms (1085 pounds) at 2.5 years of age to ~907 kilograms (2000 pounds) at 10.5 years of age,[4,5] suggesting that a considerable amount of compressive force must be absorbed during the collisions.

When bison engage in fighting, the impacts typically occur along the caudal region of the frontal bones and the interparietal bone[6] (Fig. 1.1, Fig. 2.3), and underlying these bones are the paranasal sinuses (Fig. 2.4). The paranasal sinuses are separated by bony septa that vary in their sizes and geometries, and the geometry of biological structures may be key to mitigating the energies produced during mechanical loading.[7–9] For example, the tapered spiral of the horn of a bighorn sheep ram was shown to convert the longitudinal stress wave produced when rams fight into a shear wave that dissipated at the tapered end of the horn.[7] Similarly, the curved structure of the hyoid bone of the red-bellied woodpecker also converts the longitudinal stress waves produced during drumming into shear waves;[8,9] however, models exploring the hypothesis that

the septa within the sinuses of goats act to dissipate energy have yielded varying results.[10] Models that included the septa were found to incur higher strain energies while helping to distribute stresses,[10] but in these models, strain energy was considered indicative of shock absorption;[10] whereas, in the bighorn sheep and red-bellied woodpecker models, strain energy was considered indicative of deformation or damage.[7–9] Further, well-developed sinus structures are found in bovine species that do not engage in headbutting which also suggests that the bony septa are not critical in the dissipation of impact energy, but are a vestige retained from ancestral bovines.[11]

Unlike bighorn sheep and goats that receive impacts to their horns, however, the North American bison receives blunt impacts directly to the skull; therefore, the septa may be necessary for mitigating impact energy. The mass of a bison is also significantly greater than that of a goat which suggests that the stress and strain waves produced when bison headbutt will be significantly higher than those produced when goats headbutt. Additionally, the interparietal bone of the bison skull, the location of most impacts, is thicker than the adjacent frontal bone. Theoretically, an increase in thickness should concomitantly increase the impact absorption capabilities of the interparietal bone while decreasing its susceptibility to bending.

While the macroscale septa and thickened bone structure may play a role in mitigating the energy produced when bison headbutt, the microstructure of the bone should also be noted. The bison skull contains a combination of haversian (cortical) and plexiform bone. Haversian bone behaves as transversely isotropic material, and plexiform bone behaves as an orthotropic material.[12] Additionally, plexiform bone is stiffer than haversian, and depending on its anatomical location within the bone, may have a higher elastic modulus.[12,13]

To examine how the bony septa and thickened interparietal bone within the bison skull mitigate impact energy, an FE simulation of bison headbutting was performed using variable speeds and impact locations. The resultant strain, kinetic, and internal energies were then compared and considered in the context of mitigating the energy produced when bison headbutt.

4.2 Materials and Methods

4.2.1 Mesh Generation

The FEA is based on the skull of a four-year-old male bison bull, an age considered mature for bovines,[14,15] loaned by the Museum of Vertebrate Zoology at the University of California, Berkeley (Accession number Mamm 99970). Digital Images and Communication in Medicine (DICOM) files produced by a computed tomography (CT) scan of the skull were used to render a three-dimensional model of the skull in Simpleware™ ScanIP (N-2018.03-SP2 Build 55). The resultant model was comprised of 5,186,280 triangular elements (Fig. 2.3).

To facilate the viewing of internal anatomy of the frontal and interparietal bones, decrease computational time, and to prevent the presence of islands that would compromise the FEA, the skull was halved approximately along the interfrontal suture, and the lower portion of the braincase was removed. Additionally, the nasal and incisive bones and their associated structures were also removed resulting in a model comprised of 845,460 triangular elements (Fig. 2.4). The 845,460 element model was then meshed in Simpleware™ ScanIP (N-2018.03-SP2 Build 55) using the coarsest meshing option to produce a quadratic tetrahedral mesh which was subsequently imported into Abaqus 2017 (Dassault Systèmes). The final mesh for the skull consisted of 312,726 tetrahedral quadratic C3D10M elements with an associated 534,731 nodes.

4.2.2 FEA Material Model

To simulate bison headbutting, a dynamic, explicit model using the imported meshed skull was created. The imported meshed skull was mirrored and a 4 mm thick layer of simulated ballistic gel meshed in Abaqus 2017 (Dassault Systèmes) was placed between the two skulls to approximate the presence of the scalp. The meshed gel was composed of 30,000 linear hexahedral C3D8R elements with an associated 36,057 nodes.

Using an elastic material model, the mechanical properties assigned to the skulls included values measured for a combination of haversian and plexiform bone. Material properties assigned to the skull include a modulus of 12,400 MPa,[16] a density of 2.06 E-9 tonnes,[13,16] and a Poisson's ratio of 0.34[17] (Table 4.1). The material properties assigned to the ballistic gel include a modulus of 210 MPa,[18] a density of 1.25 E-12 (based on data from Datoc),[19] and a Poisson's ratio of 0.3[18] (Table 4.1).

Although the modulus of bone can vary based on its location, a single modulus was applied to the models based on the results of the histology analysis. The histology of the interparietal and frontal bones was found to be a combination of haversian and plexiform bone, and all samples showed similar interspersion of the bone types; therefore, the use of a single modulus is valid. Additionally, the density and thickness assigned to the ballistic gel are somewhat low, but the modulus should be high enough to provide enough stiffness to offset any density or thickness effects.

4.2.3 FEA Boundary Conditions

The left skull receiving the impact (opponent) was encastred along the bottom surface, while an instantaneous velocity was applied to the right skull initiating the impact (aggressor)

(Figs. 4.1-4.4). Due to some confusion over the speed at which bison collide when fighting (e.g. Fuller),[2] four different velocities were applied: 2235.2 mm/s, 6705.6 mm/s, 11176 mm/s, and 13411 mm/s. The impact location was also varied among three locations: contact between midfrontal region of the aggressor and the midfrontal region of the opponent (midfrontal-midfrontal), contact between the interparietal bones of the aggressor and opponent (interparietal-interparietal), and contact between the interparietal bone of the aggressor and the midfrontal region of the opponent (oblique).

4.2.4 Data Analysis

The von Mises stress contours were plotted using an upper limit of 294 MPa, the compressive strength of plexiform bone.[20] Strain, kinetic, and the internal energy resulting from the initial impact were used as metrics for the analysis.[7] To assess the relative contribution of each velocity and each impact location on the resultant strain energy for each model, a principal components analysis (PCA) of the covariance matrix was performed using OriginPro, Version 2019 (OriginLab Corporation, Northampton, Massachusetts).

4.3 Results

4.3.1 FEA

The von Mises stress contours for the initial impact and midpoints of each model are presented in Figs. 4.1-4.4. Based on the stress contours, as impact velocity increases, the stress increases with the highest global stresses occurring during oblique impacts. The stress tends to be distributed about the skull in the interparietal-interparietal impacts, but focal stress concentrations are produced at the impact location in midfrontal-midfrontal and oblique impacts.

None of the models exhibit global stresses in excess of the compressive strength of plexiform bone. Because the skull of the competitor was encastred along bottom edge, the maximum stress value given in the contour plots may not accurately reflect the true maximum stress due to reflection of the stress wave by the encastred region.

4.3.2 Data Analysis

Across all models, the strain and internal energies increase as the impact velocity increases. The kinetic energy for all models is inversely proportional to the internal energy. Oblique impacts produce the greatest strain energies while interparietal-interparietal impacts produce the lowest strain energies (Tables 4.2-4.4; Figs. 4.5-4.8).

The results of the PCA suggest that the impact speed contributes the most variation to the resultant strain energy for each model followed by impact location. Impact velocity lies along Principal Component axis 1 (PC1), and accounts for 92.39% of the variation in strain energy among models, while the impact locations lie along PC2 and account for 7.59% of the variation among models. Among the impact locations, oblique impacts contribute the most variance, followed by midfrontal-midfrontal impacts, and finally interparietal-interparietal impacts (Table 4.5; Figs. 4.9-4.14).

4.4. Discussion and Conclusions

Based on the trends in the data, interparietal-interparietal impacts, of which the bison naturally partake, produce the least amount of strain energy, indicating that impacts at this location result in less associated deformation. Further, the impact energy produced during the interparietal-interparietal collisions tends to be lower and dispersed about the skull; whereas, in midfrontal-midfrontal and oblique collisions, localized stress concentrations occur at the impact

location; however, of note, global stresses did not exceed the compressive strength of plexiform bone regardless of impact velocity or location. Additionally, the interparietal bone tends to be thicker than the frontal bone and may provide more efficient energy absorption and dispersion than that of the frontal bone.

Assessing the energy dissipation capabilities of the bony septa that underlie the frontal and interparietal bones is difficult. While some of the septa are tapered, the gross geometries of the septa vary within the skull and can vary among individuals making them difficult to compare to the energy dissipation provided by the taper of the horn of a ram.[7,21] Based on an FEA of goats headbutting[10] and the morphology of Bovidae sinuses[11], hypotheses exist that the bony septa serve to store strain energy and are not an adaptation to facilitate headbutting;[10,11] but the validity of these hypotheses is also unclear based on the current model and should be further explored. In bison, it is likely that the thickness of the interparietal bone works in concert with the geometries of the bony septa to prevent local stress concentrations through effective absorption and dispersion of the blunt impact energy produced during headbutting.

The models employed in these analyses have limitations. Future models will include a comparison of the energies produced when bison headbutt to that of the energies produced in a theoretical model of the domestic cow headbutting. To account for the mass of the bison and to prevent the reflection of the stress wave along an encastred surface, a connector or spring will be added to the left skull to facilitate movement. An additional model, where the bony septa are removed from the bison skull, will also be tested. The material properties of the model will also be adjusted to make the ballistic gel thicker and denser, and a viscoelastic damage model will also be employed. Additionally, the atlas and axis (first two cervical vertebrae) of the bison will be simulated to test the hypothesis that owing to the dense nature of these vertebrae, they act as

shock absorbers during headbutting.[6] Finally, the microarchitecture of the haversian-plexiform mixture of bone found in the bison skull will be further examined to determine its contribution to energy dissipation. Such improvements should help delineate the importance of material thickness and geometry on energy dissipation.

Based on the current model, it may be inferred that the bison skull is strategically thickened in areas that experience blunt impact preventing the focal concentration of stress. Strategic thickening or strategically placing shock absorbing materials in safety equipment is a possibility for improving its efficacy – provided the weight of the equipment is not significantly increased. Manufacturers currently produce sports helmets that employ the strategic placement of shock absorption materials,[22] and as models and the understanding of natural impact systems, such as that of the North American bison skull, improve, designs and materials that are efficacious in mitigating blunt impact injuries will evolve.

Table 4.1
Material Properties Assigned to the Bison Skull and Ballistic Gel

	Skull	Gel
Modulus (MPa)	12,400[16]	210[18]
Density (Tonnes)	2.06E-09[13,16]	1.25E-12[19]
Poisson's Ratio	0.34[17]	0.3[18]

Table 4.2
Strain Energy Produced upon Initial Impact for Each Speed and Impact Location

	2235.2 mm/s	6705.g mm/s	11176 mm/s	13411 mm/s
Interparietal-Interparietal	1230.3	10775.3	27309.7	36375.3
Midfrontal-Midfrontal	1301	10423.3	35434.7	54944.7
Oblique	1799.34	16111.2	43530.6	59981.5

Table 4.3
Kinetic Energy Value of the Initial Impact for Each Speed and Impact Location

	2235.2 mm/s	6705.g mm/s	11176 mm/s	13411 mm/s
Interparietal-Interparietal	3126.56	28280.3	79260.2	114086
Midfrontal-Midfrontal	3019.29	28635.3	70049.3	97921.6

Oblique	2518.41	22770.3	64251.4	95235.6

Table 4.4
Internal Energy Value of the Initial Impact for Each Speed and Impact Location

	2235.2 mm/s	**6705.g mm/s**	**11176 mm/s**	**13411 mm/s**
Interparietal-Interparietal	1283.27	11537	29613.3	41210.5
Midfrontal-Midfrontal	1356.27	10704.2	36358.9	56130
Oblique	1969.99	16602.1	43788.1	60296.9

Table 4.5
Extracted Eigenvalues for Principal Component Axes 1 and 2

	Extracted Eigenvalues	**Extracted Eigenvalues**
	(PC1 = 92.39%)	**(PC2 = 7.59%)**
Velocity	0.87591	-0.48015
Interparietal-Interparietal	0.18957	0.39101
Midfrontal-Midfrontal	0.30842	0.4834
Oblique	0.31894	0.61879

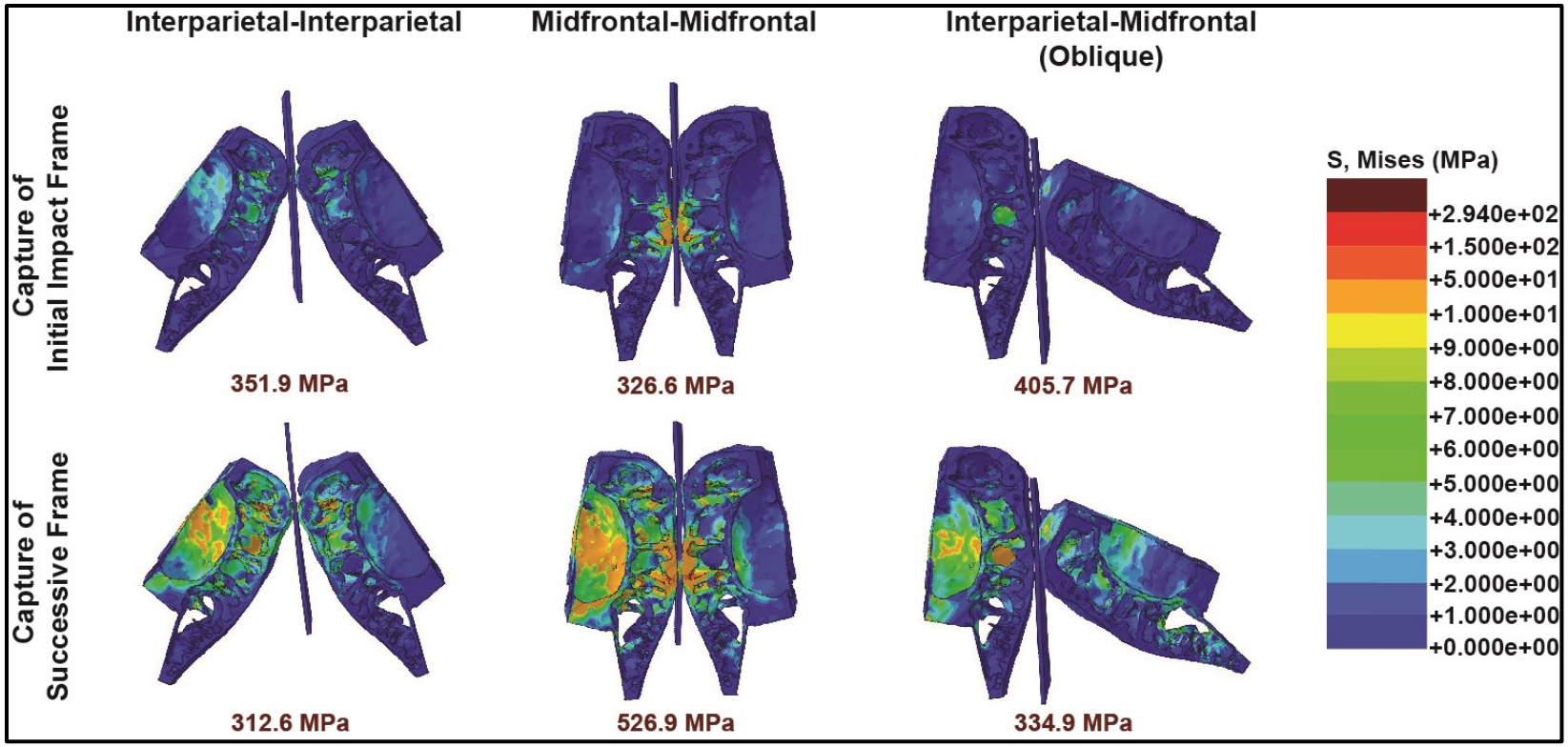

Figure 4.1 Comparison of the stresses incurred at each impact location when the instantaneous velocity equals 2235.2 mm/s.

The top row represents is a capture of the initial impact, and the bottom row is a capture of the frame immediately after the initial impact. In all models, the aggressor is on the right, and the opponent is on the left. Stress values given below each model represent the maximum stress incurred by an element in that particular frame. Note that the stress is concentrated in the opponent due to reflection of the shockwave from the encastred portion of the skull; therefore, the maximum stress reported on the scale may reflect the concentrated value.

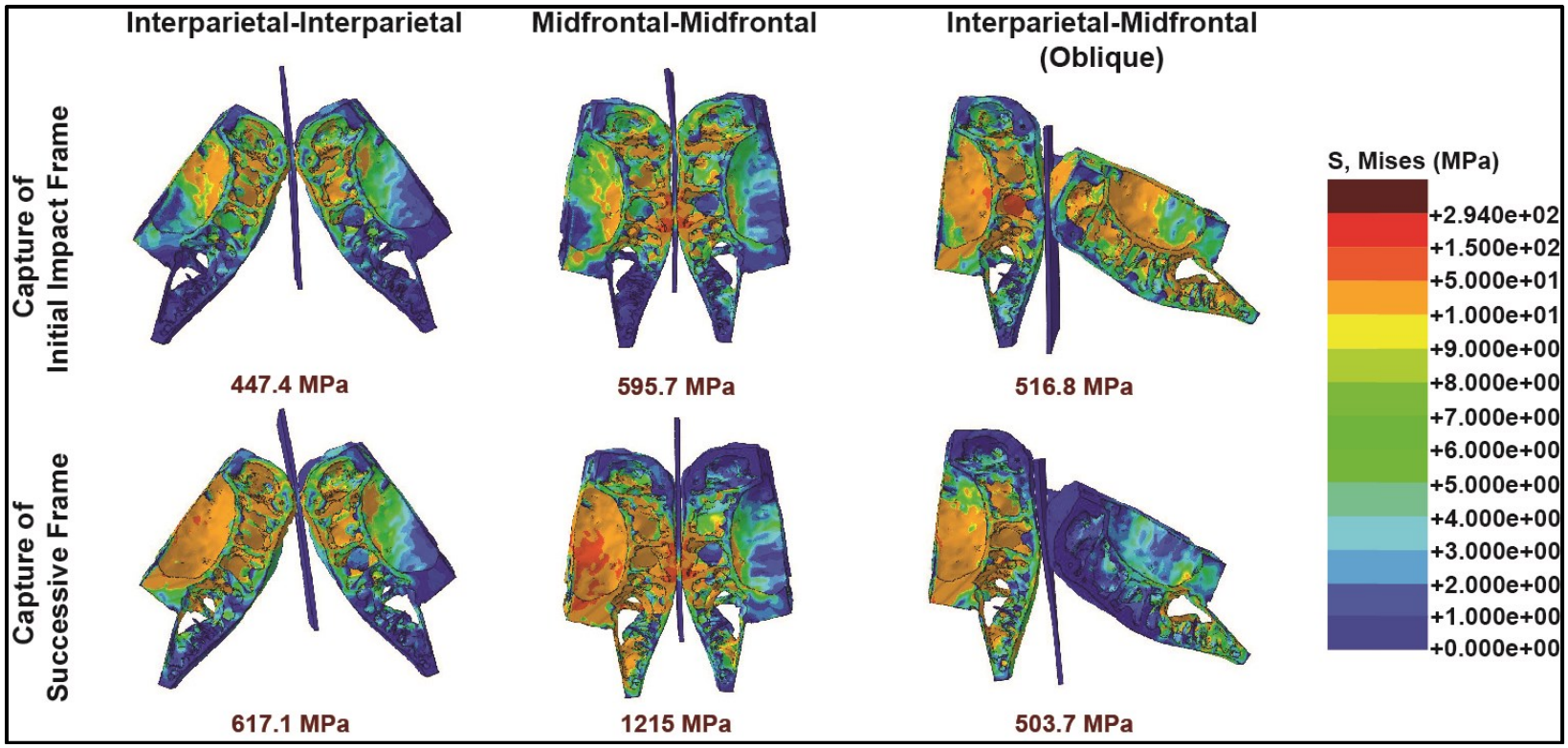

Figure 4.2 Comparison of the stresses incurred at each impact location when the instantaneous velocity equals 6705.6 mm/s.

The top row represents is a capture of the initial impact, and the bottom row is a capture of the frame immediately after the initial impact. In all models, the aggressor is on the right, and the opponent is on the left. Stress values given below each model represent the maximum stress incurred by an element in that particular frame. Note that the stress is concentrated in the opponent due to reflection of the shockwave from the encastred portion of the skull; therefore, the maximum stress reported on the scale may reflect the concentrated value.

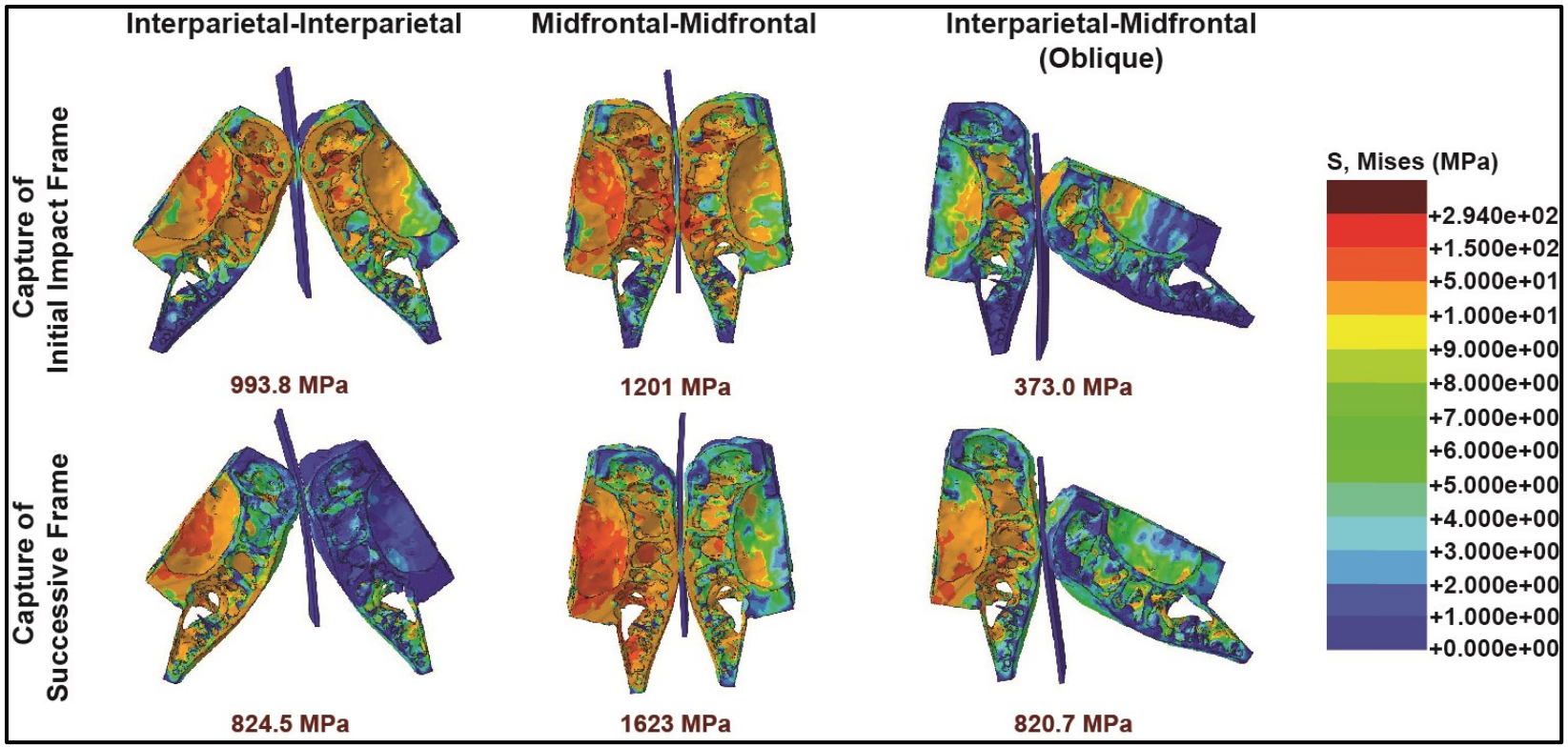

Figure 4.3 Comparison of the stresses incurred at each impact location when the instantaneous velocity equals 11176 mm/s.

The top row represents is a capture of the initial impact, and the bottom row is a capture of the frame immediately after the initial impact. In all models, the aggressor is on the right, and the opponent is on the left. Stress values given below each model represent the maximum stress incurred by an element in that particular frame. Note that the stress is concentrated in the opponent due to reflection of the shockwave from the encastred portion of the skull; therefore, the maximum stress reported on the scale may reflect the concentrated value.

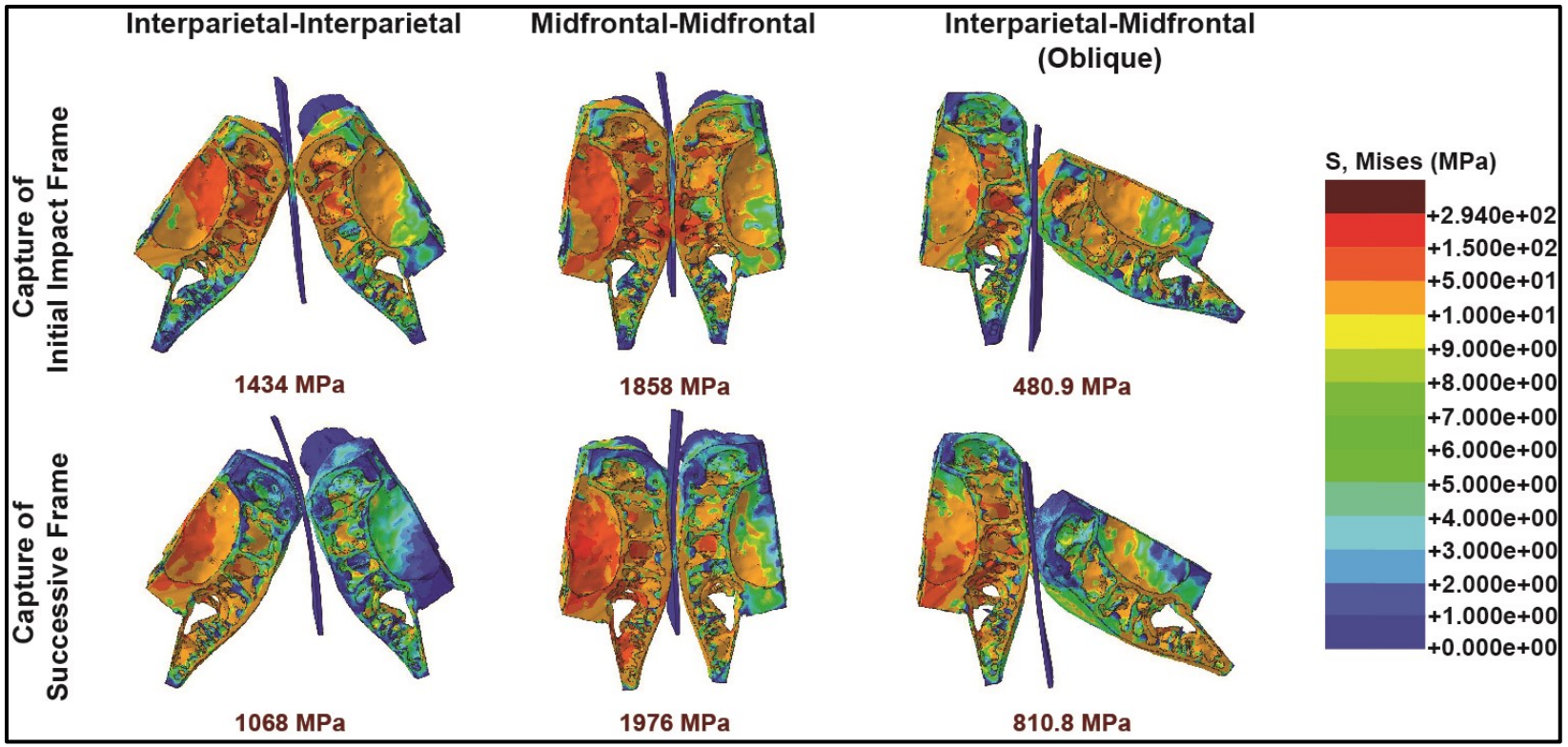

Figure 4.4 Comparison of the stresses incurred at each impact location when the instantaneous velocity equals 13411 mm/s.

The top row represents is a capture of the initial impact, and the bottom row is a capture of the frame immediately after the initial impact. In all models, the aggressor is on the right, and the opponent is on the left. Stress values given below each model represent the maximum stress incurred by an element in that particular frame. Note that the stress is concentrated in the opponent due to reflection of the shockwave from the encastred portion of the skull; therefore, the maximum stress reported on the scale may reflect the concentrated value.

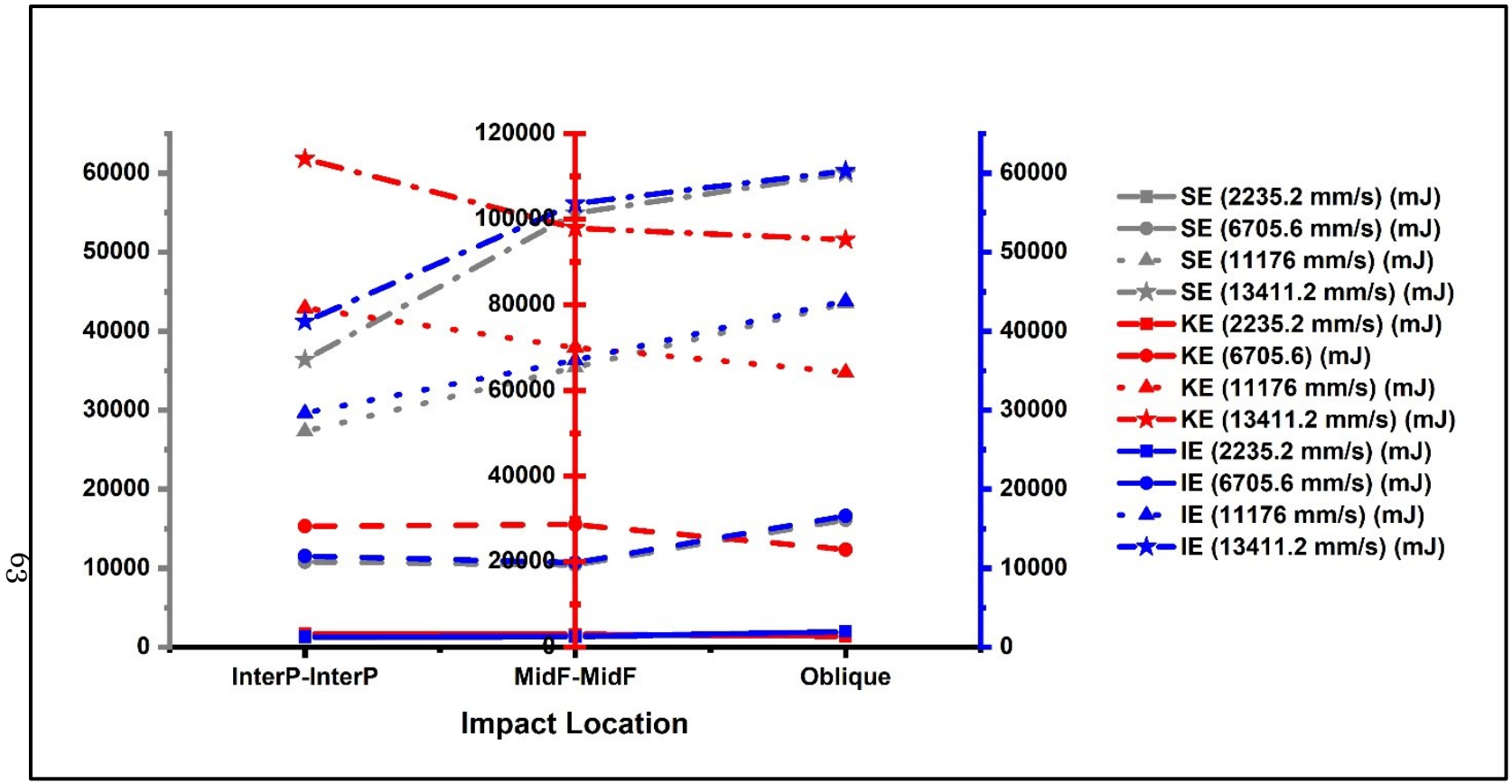

Figure 4.5 Comparison of the strain, kinetic, and internal energies across all models.

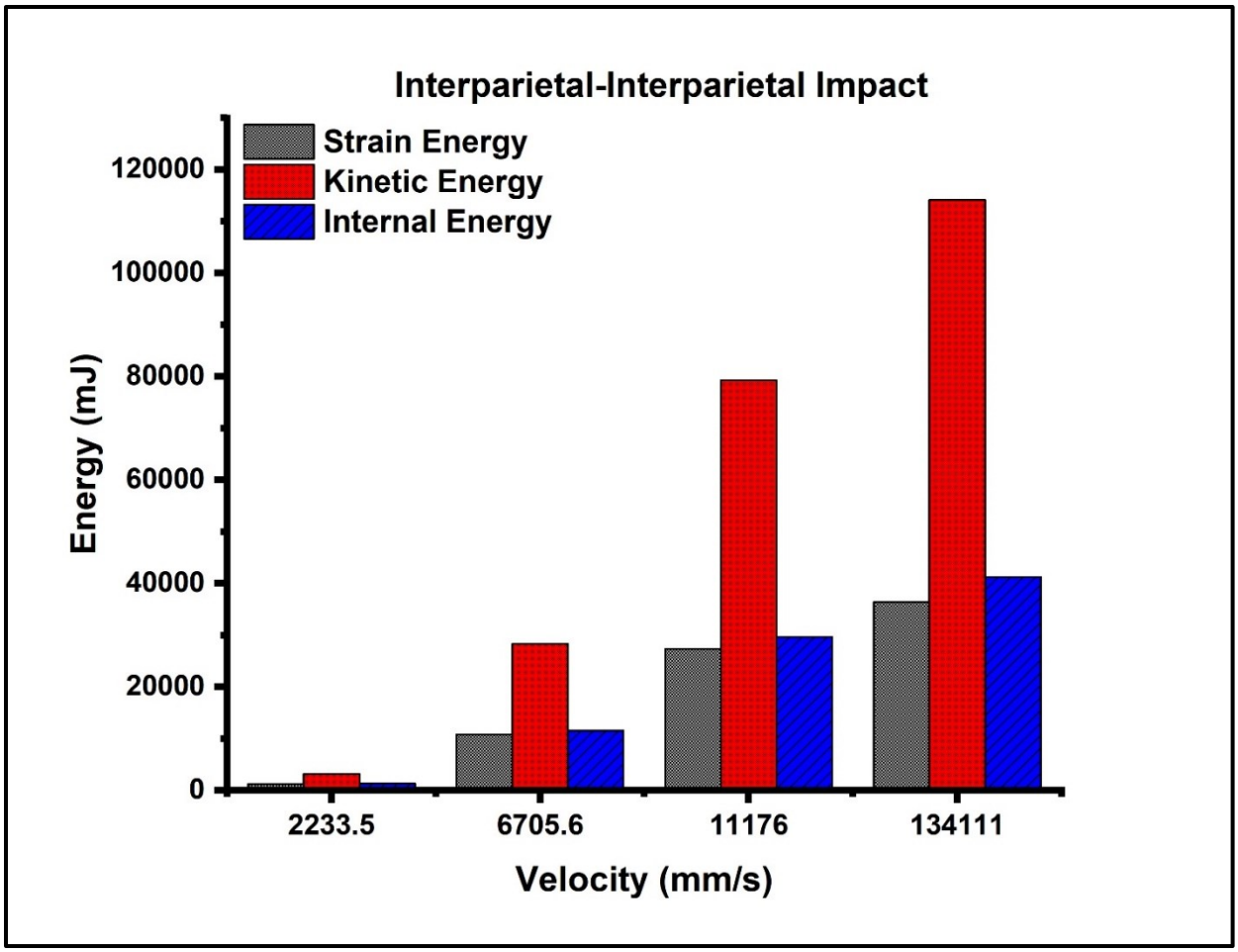

Figure 4.6 Comparison of the strain, kinetic, and internal energies for interparietal-interparietal impacts at each velocity.

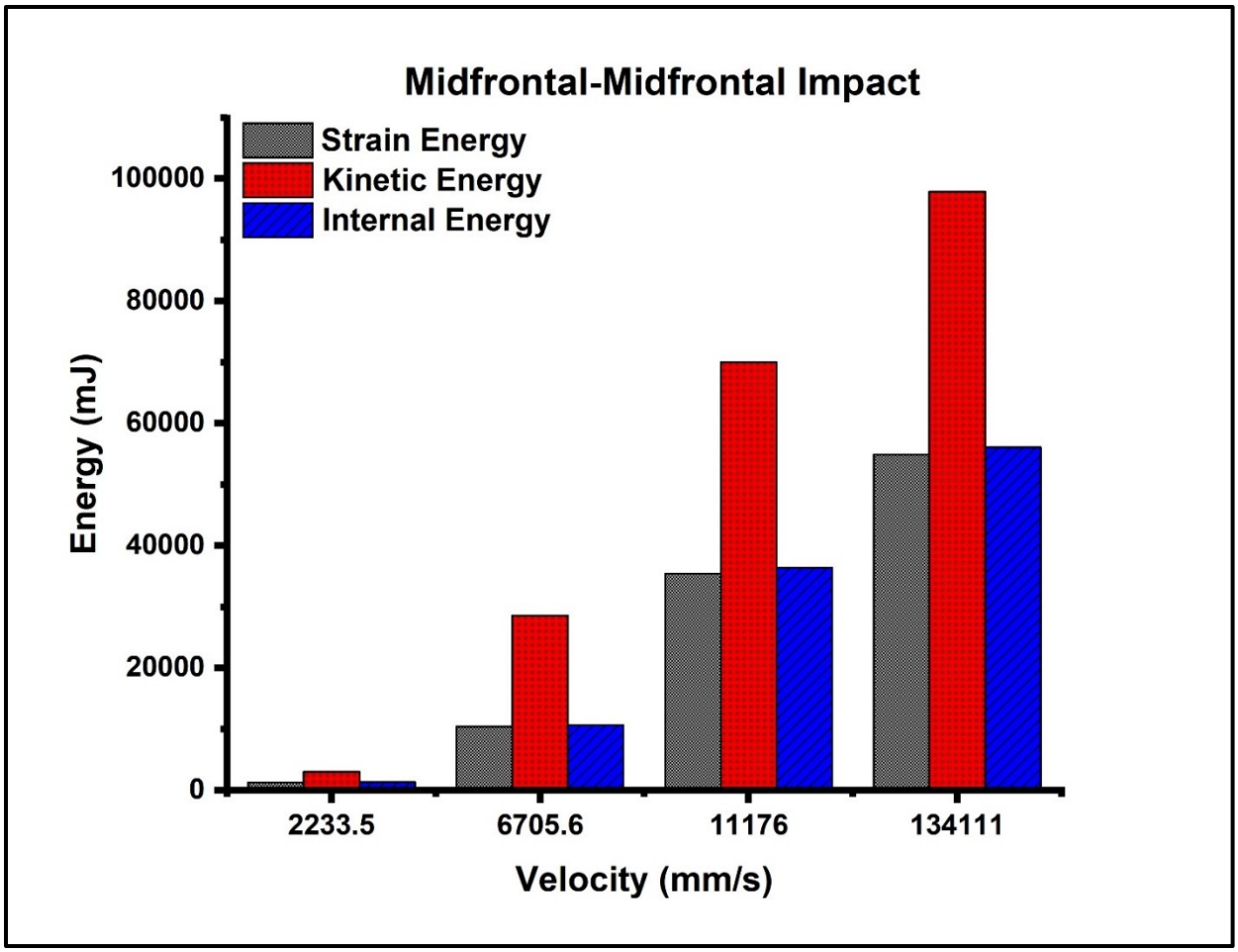

Figure 4.7 Comparison of the strain, kinetic, and internal energies for midfrontal-midfrontal impacts at each velocity.

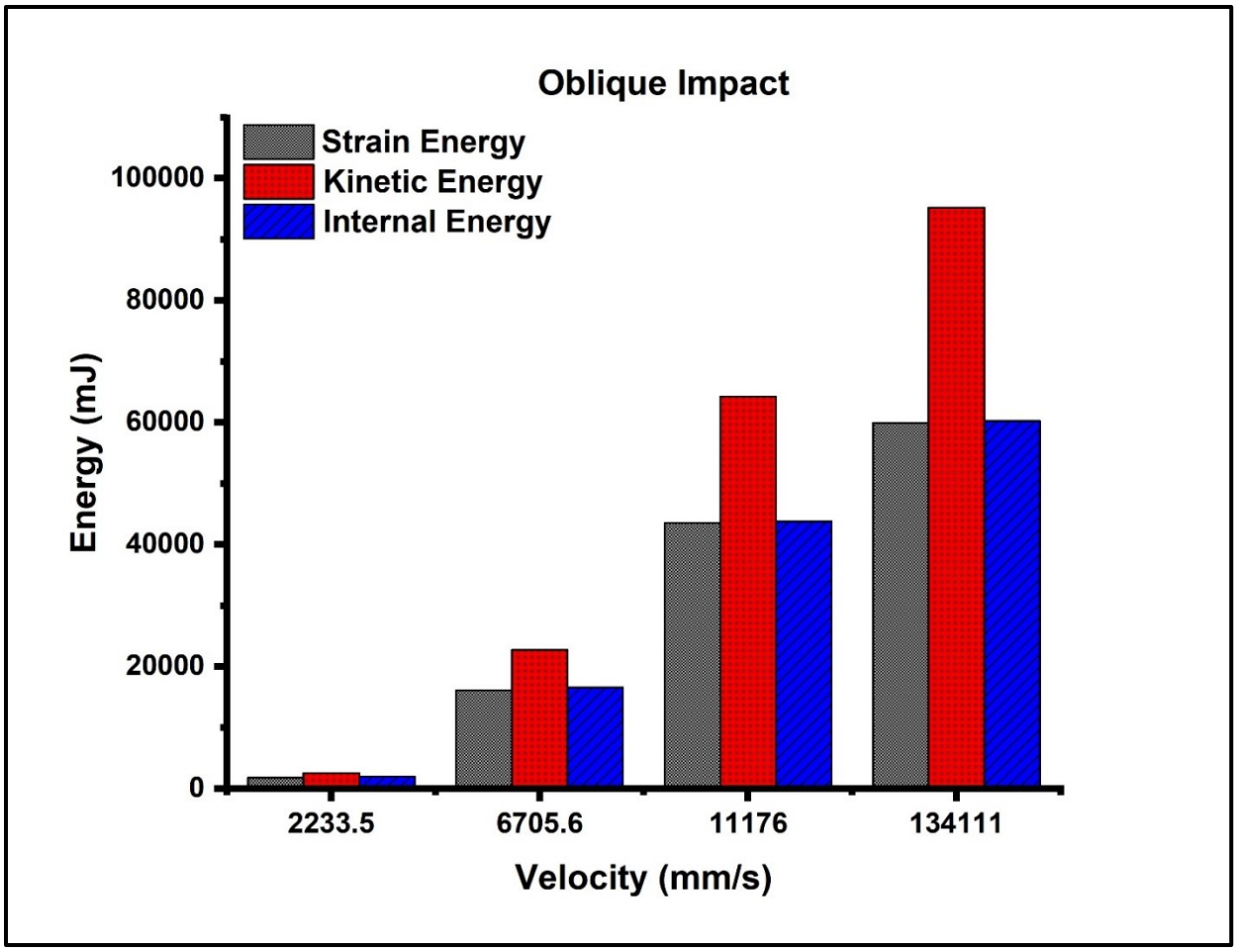

Figure 4.8 Comparison of the strain, kinetic, and internal energies for oblique impacts at each velocity.

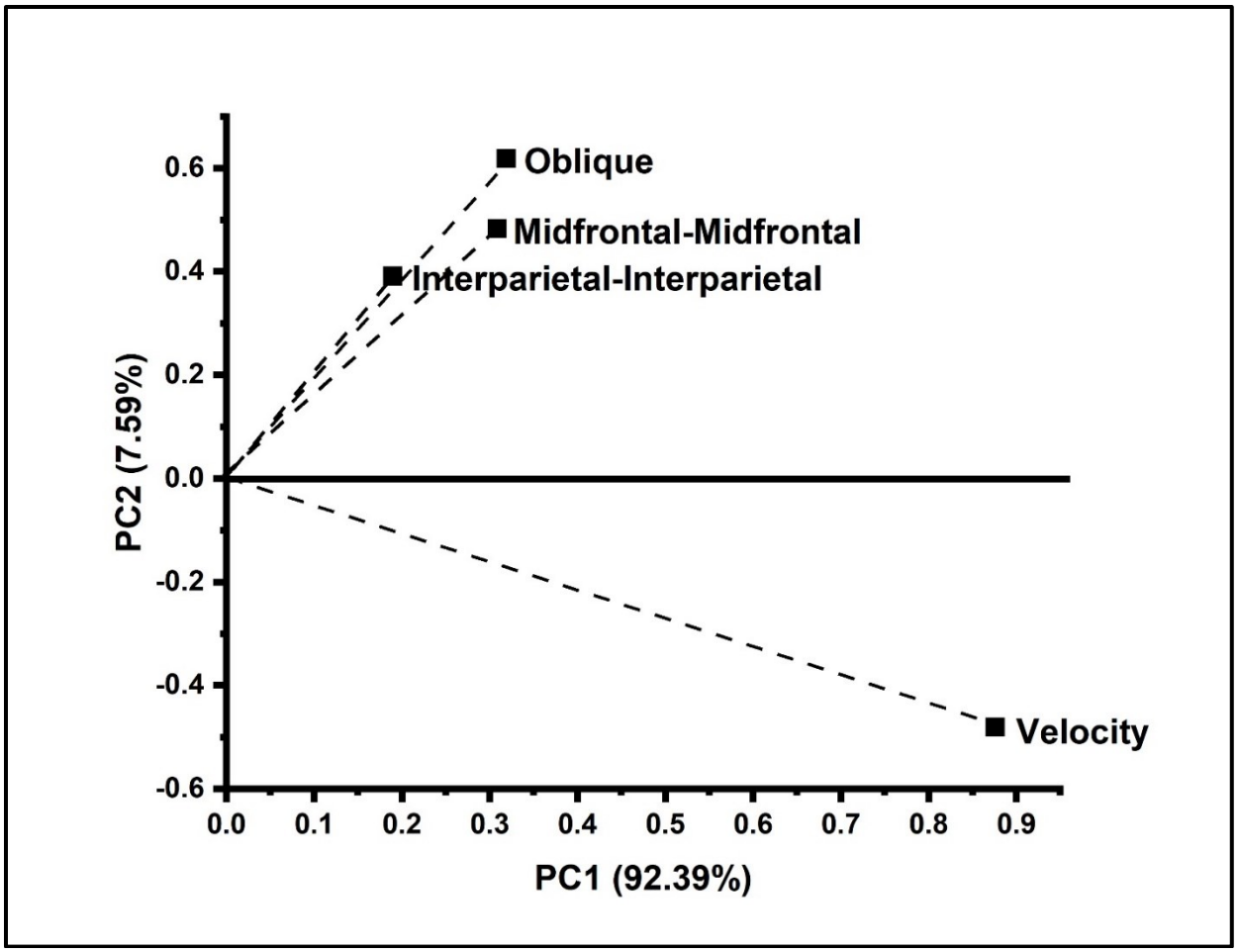

Figure 4.9 Principal Component Analysis (PCA) loading plot of the covariance matrix of strain energy. Principal component axis 1 is dominated by velocity while principal component axis 2 is dominated by impact location.

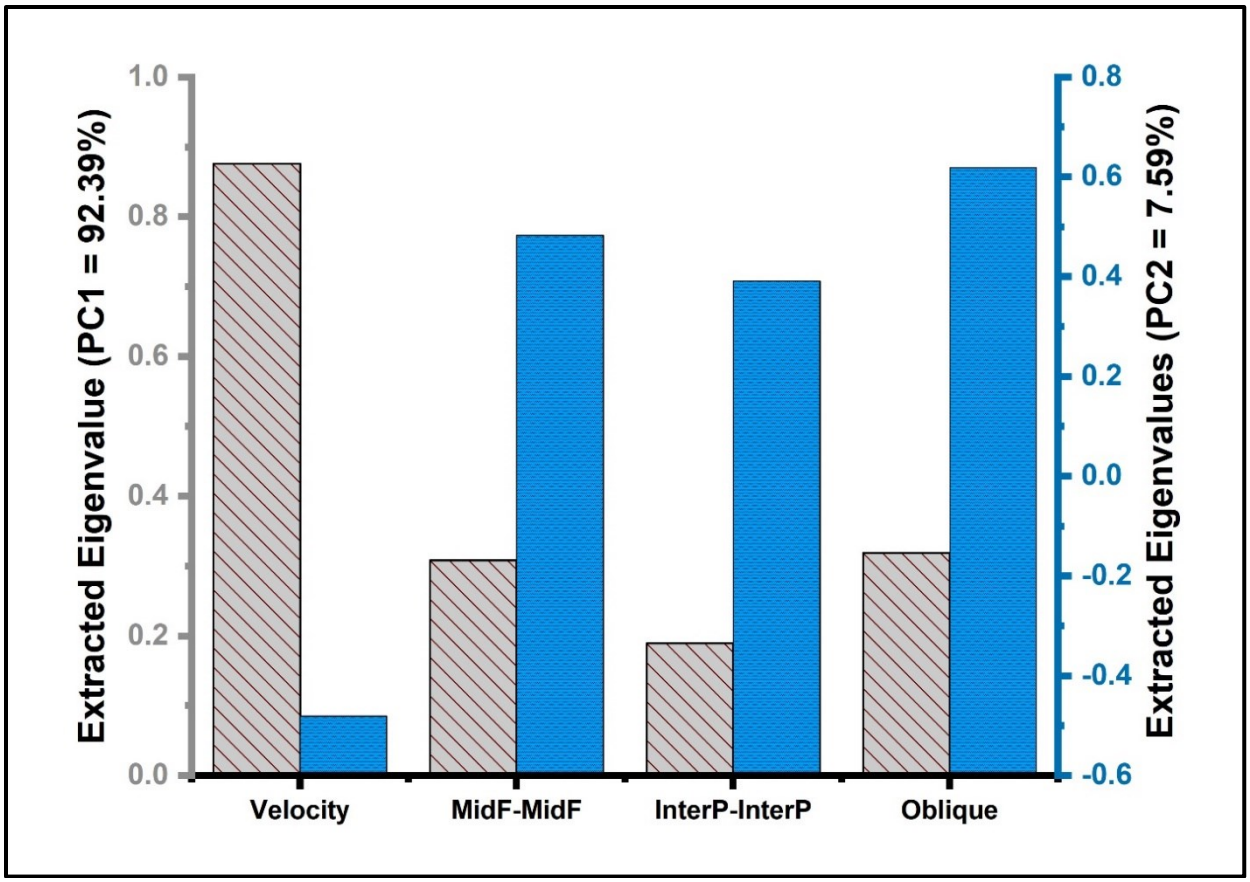

Figure 4.10 Comparison of the extracted eigenvalues from the PCA of strain energy. The second axis is dominated by the impact location with oblique impacts accounting for the majority of the variance.

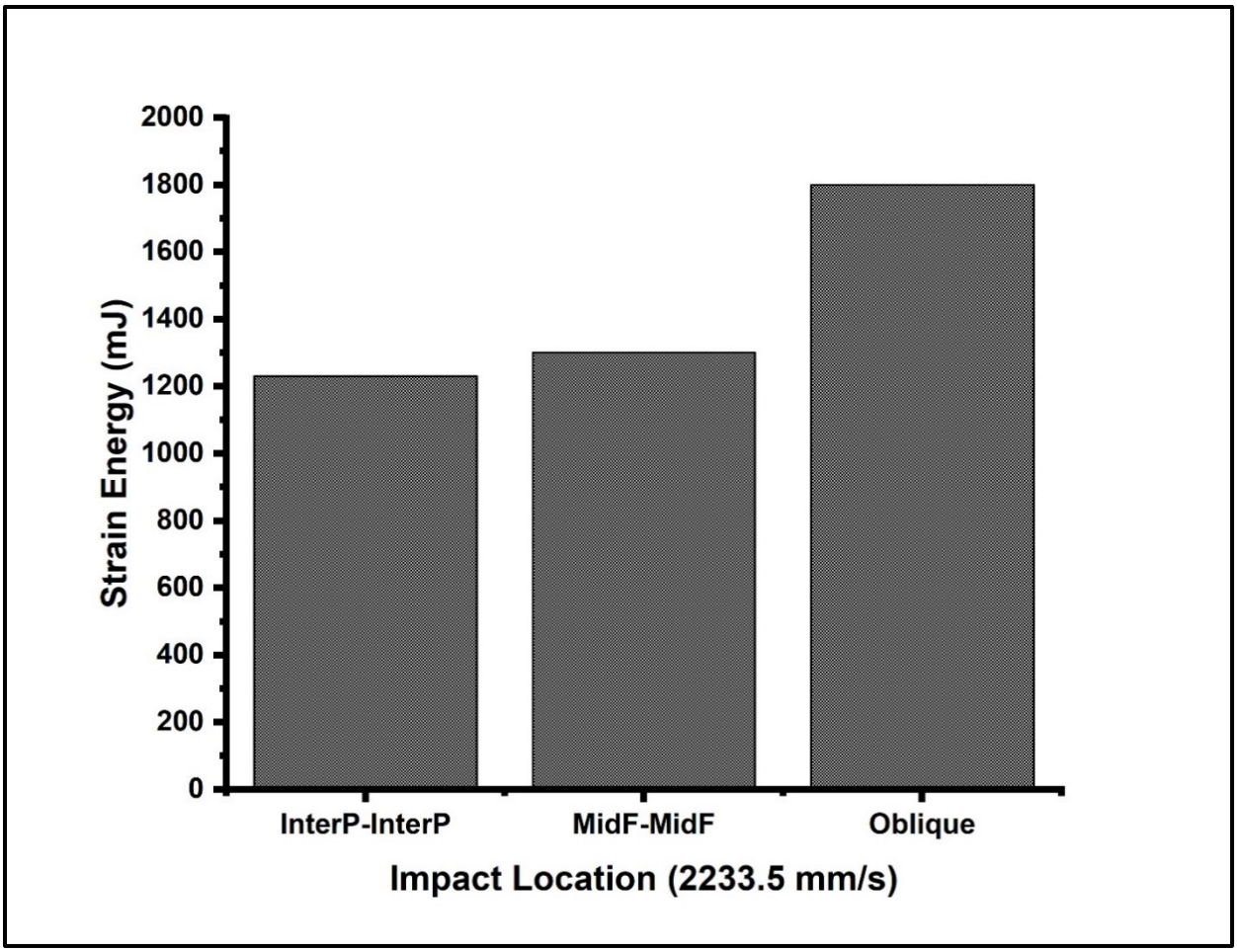

Figure 4.11 Comparison of the strain energy produced at each location at an impact velocity of 2233.5 mm/s. The highest strain energy is produced by the oblique impact.

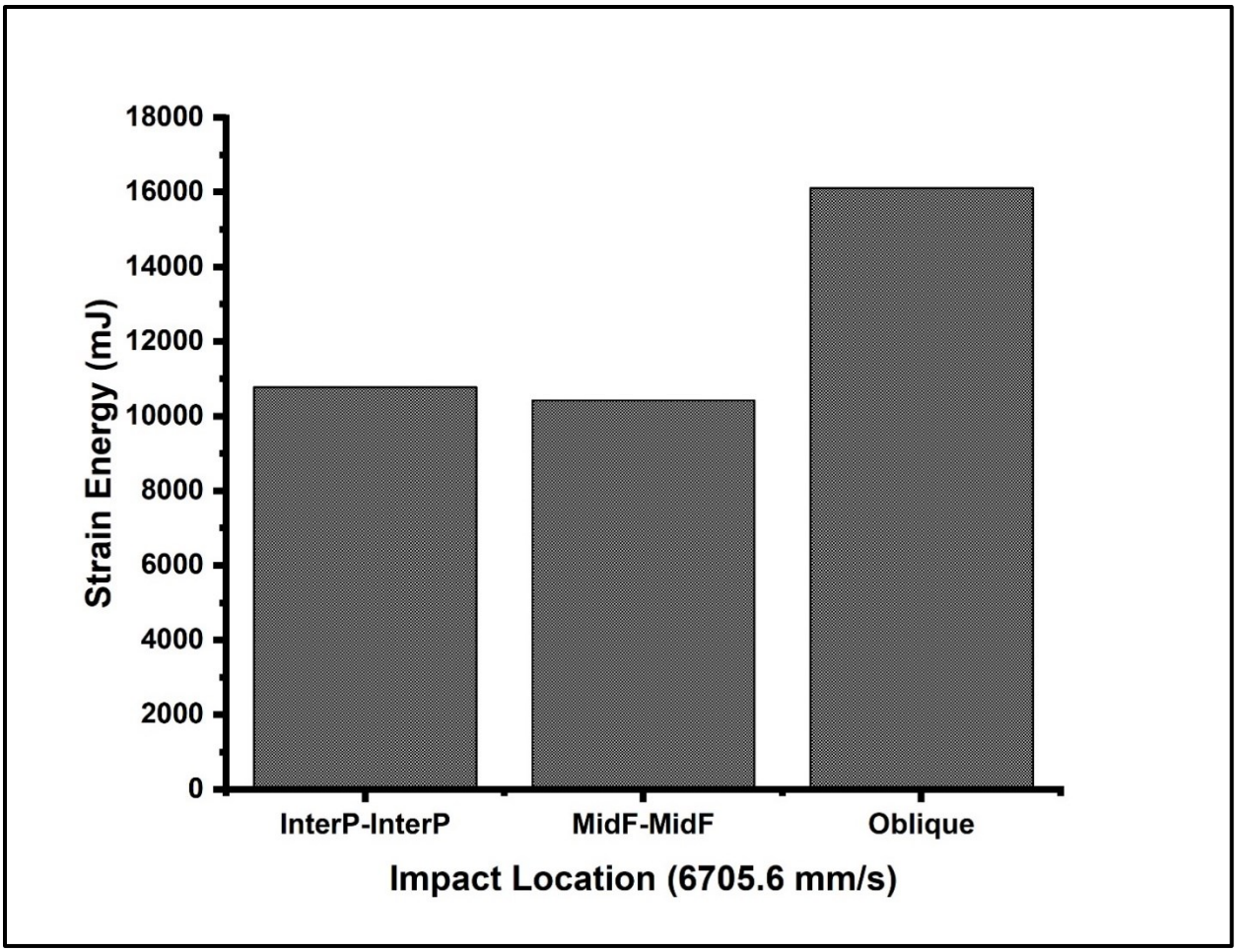

Figure 4.12 Comparison of the strain energy produced at each location at an impact velocity of 6705.6 mm/s. The highest strain energy is produced by the oblique impact.

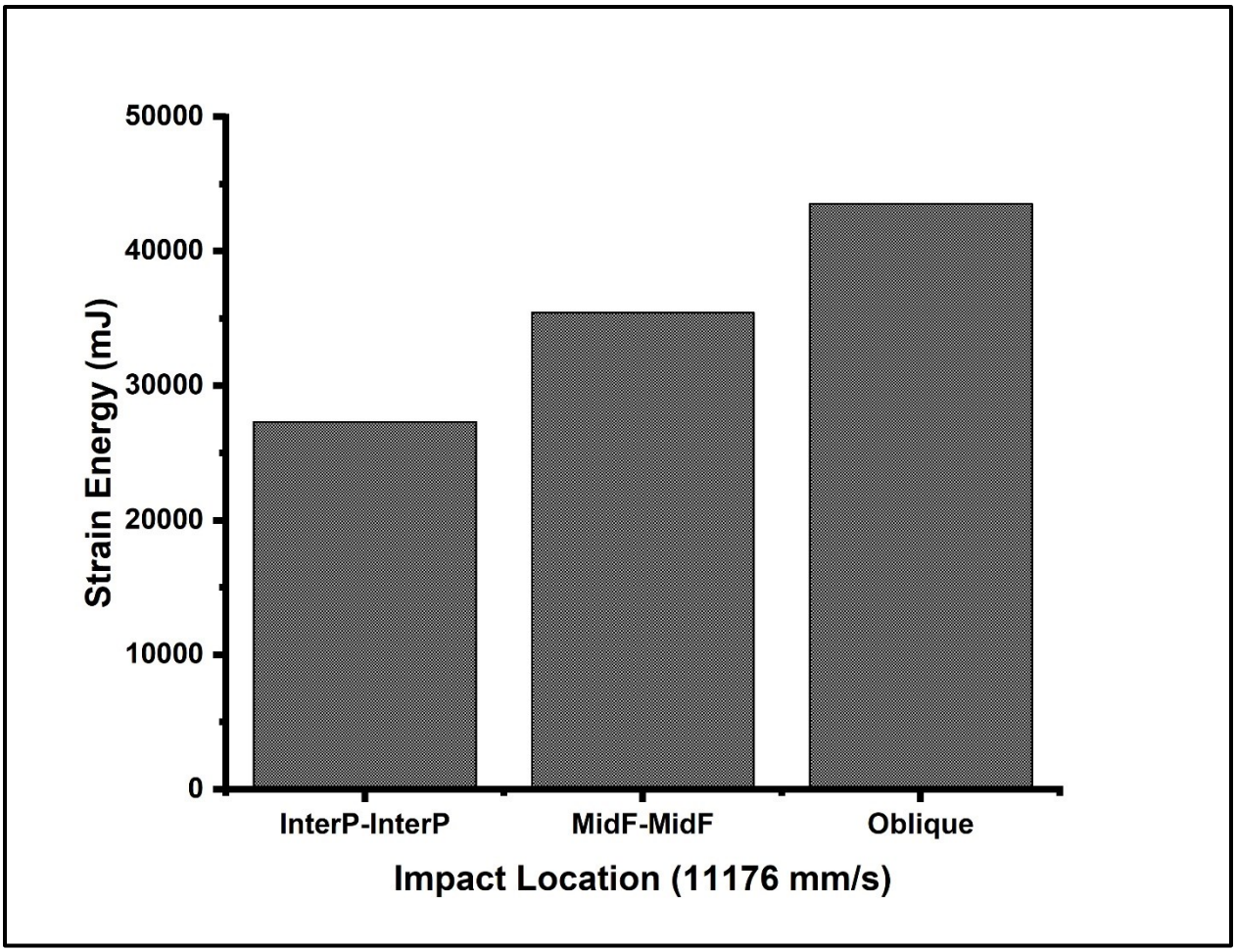

Figure 4.13 Comparison of the strain energy produced at each location at an impact velocity of 11176 mm/s. The highest strain energy is produced by the oblique impact.

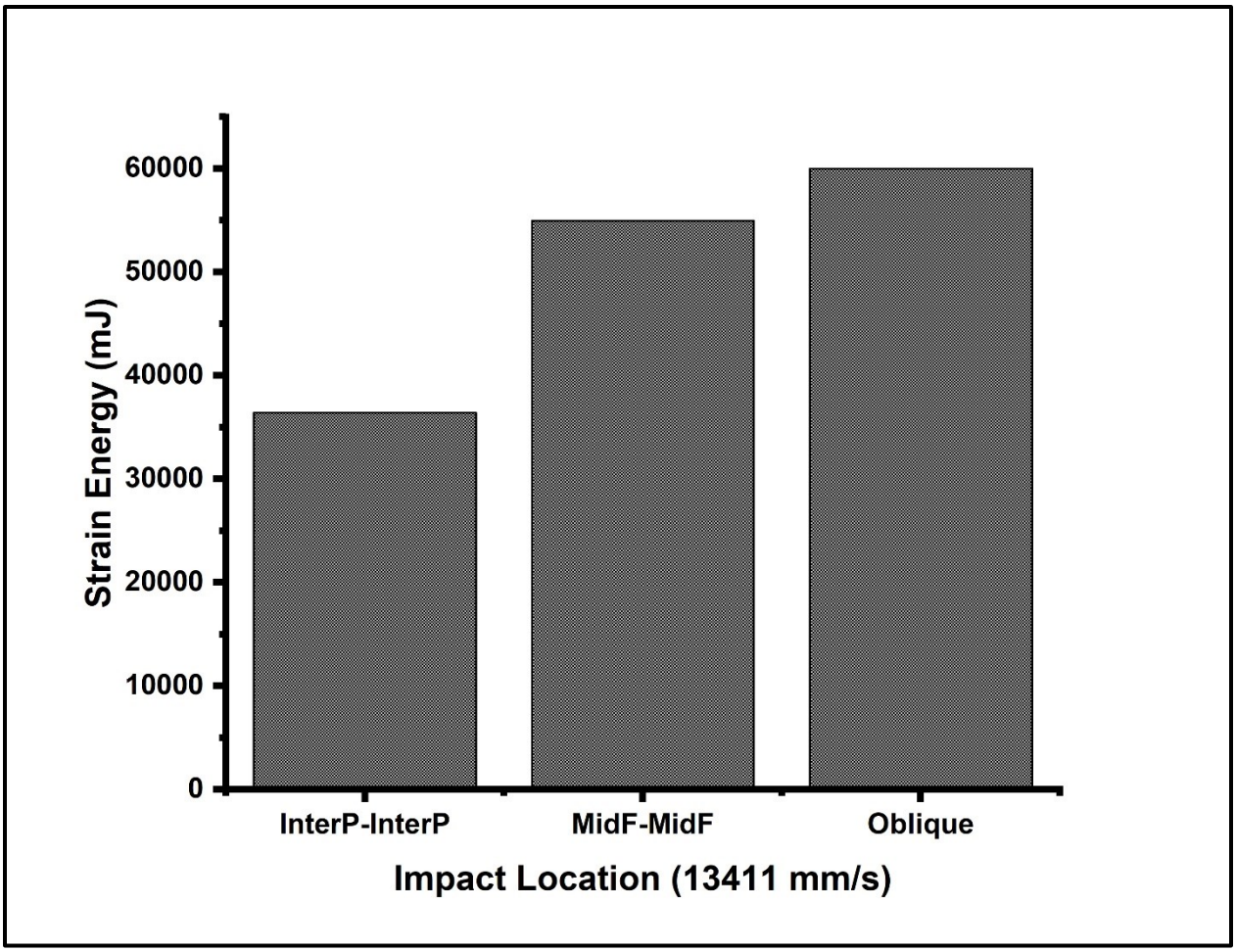

Figure 4.14 Comparison of the strain energy produced at each location at an impact velocity of 13411 mm/s. The highest strain energy is produced by the oblique impact.

References

1. McHugh T. Social behavior of the American buffalo (*Bison bison bison*). *Zoologica : scientific contributions of the New York Zoological Society*. 1958;43(1):1-40.

2. Fuller WA. Behaviour and Social Organization of the Wild Bison of Wood Buffalo National Park, Canada. *1*. 1960;13(1):2-19. doi:10.14430/arctic3685

3. Lott DF. Sexual and Aggressive Behavior of Adult Male American Bison (*Bison bison*) in The Behaviour of Ungulates and its relation to management. *IUCN Publications new series*. 1974;I(24):382-394.

4. Lott DF. *American Bison, A Natural History*. University of California Press; 2002.

5. Licht DS. Bison Weights From National Parks in the Northern Great Plains. *Rangelands*. 2016;38(3):138-144. doi:10.1016/j.rala.2016.02.003

6. Kreutzer LA. Bison and deer bone mineral densities: Comparisons and implications for the interpretation of archaeological faunas. *Journal of Archaeological Science*. 1992;19(3):271-294. doi:10.1016/0305-4403(92)90017-W

7. Johnson KL, Trim MW, Horstemeyer MF, et al. Geometric Effects on Stress Wave Propagation. *J Biomech Eng*. 2014;136(2):021023-021023-12. doi:10.1115/1.4026320

8. Lee N, Horstemeyer MF, Rhee H, Nabors B, Liao J, Williams LN. Hierarchical multiscale structure–property relationships of the red-bellied woodpecker (*Melanerpes carolinus*) beak. *Journal of The Royal Society Interface*. 2014;11(96):20140274. doi:10.1098/rsif.2014.0274

9. Lee N, Horstemeyer MF, Prabhu R, et al. The geometric effects of a woodpecker's hyoid apparatus for stress wave mitigation. *Bioinspir Biomim*. 2016;11(6):066004. doi:10.1088/1748-3190/11/6/066004

10. Farke AA. Frontal sinuses and head-butting in goats: a finite element analysis. *Journal of Experimental Biology*. 2008;211(19):3085-3094. doi:10.1242/jeb.019042

11. Farke AA. Evolution and functional morphology of the frontal sinuses in Bovidae (Mammalia: Artiodactyla), and implications for the evolution of cranial pneumaticity. *Zool J Linn Soc*. 2010;159(4):988-1014. doi:10.1111/j.1096-3642.2009.00586.x

12. Katz JL, Yoon HS. The structure and anisotropic mechanical properties of bone. *IEEE Trans Biomed Eng*. 1984;31(12):878-884. doi:10.1109/TBME.1984.325252

13. Martin RB, Boardman DL. The effects of collagen fiber orientation, porosity, density, and mineralization on bovine cortical bone bending properties. *Journal of Biomechanics*. 1993;26(9):1047-1054. doi:10.1016/S0021-9290(05)80004-1

14. Carter DR, Hayes WC, Schurman DJ. Fatigue life of compact bone—II. Effects of microstructure and density. *Journal of Biomechanics*. 1976;9(4):211-218. doi:10.1016/0021-9290(76)90006-3

15. Manilay Z, Novitskaya E, Sadovnikov E, McKittrick J. A comparative study of young and mature bovine cortical bone. *Acta Biomaterialia*. 2013;9(2):5280-5288. doi:10.1016/j.actbio.2012.08.040

16. Novitskaya E, Chen P-Y, Lee S, et al. Anisotropy in the compressive mechanical properties of bovine cortical bone and the mineral and protein constituents. *Acta Biomaterialia*. 2011;7(8):3170-3177. doi:10.1016/j.actbio.2011.04.025

17. Van Buskirk WC, Cowin SC, Ward RN. Ultrasonic measurement of orthotropic elastic constants of bovine femoral bone. *J Biomech Eng*. 1981;103(2):67-72. doi:10.1115/1.3138262

18. Al Khalil M, Frissane H, Taddei L, et al. SPH-based method to simulate penetrating impact mechanics into ballistic gelatin: Toward an understanding of the perforation of human tissue. *Extreme Mechanics Letters*. 2019;29:100479. doi:10.1016/j.eml.2019.100479

19. Datoc D. Finite Element Analysis and Modeling of a .38 Lead Round Nose Ballistic Gelatin Test. April 2010. https://digitalcommons.calpoly.edu/theses/274.

20. Cow Compact Bone, Fibrolamellar. http://www.matweb.com/search/datasheet.aspx?MatGUID=e312f442ba2942e88ba30ec764d0ff8c. Accessed October 17, 2019.

21. Budras K-D, Habel RE, Mülling CKW, Greenough PR, eds. *Bovine Anatomy*. Second. Schlütersche; 2011.

22. The S Lacrosse Helmet | High Performance Men's Lacrosse Helmet. *Cascade*. https://cascadelacrosse.com/product/mens-lacrosse-helmets-the-s/. Accessed October 18, 2019.